/N - 39

58527

P-59

Structural Properties of Impact Ices
Accreted on Aircraft Structures

R.J. Scavuzzo and M.L. Chu
The University of Akron
Akron, Ohio

January 1987

NASA
National Aeronautics and
Space Administration

1.0 Introduction

The formation of ice on engines and airfoils of fixed wing aircraft and helicopter blades can seriously degrade the safety of an aircraft. On fixed wing aircraft ice deposits adversely affect the acrodynamic characteristics of engines and airfoils. Ice accumulation on helicopter rotor blades is an especially serious problem. In addition the blade can become unbalanced if the ice sheds unevenly causing dangerous vibration. Furthermore ice shed from aircraft surfaces can fly into an engine and destroy some blades.

Typical ice accretions on an airfoil are shown on Figure 1. Ice conditions were varied to form an ice cap of clear glaze ice (a), mixed glaze and rime ice regions. (b) and white rim ice (c). Downstream of the ice cap, separate ice finger on glaze or rime ice form. Back lighted photographs of these ice conditions are shown in Figure 2. Rime ice forms as partially sintered fingers that grow up-trajectory as shown on Figure 3. It is suspected that the tensile strength perpendicular to the fingers of rime ice is very small. Aircraft deicing systems must obviously be able to clearly shed ice which varies significantly in mechanical properties.

Three basic categories of deicing systems are used to deice aircraft or other structures: mechanical systems, thermal systems and chemical systems.

Some mechanical systems used or considered for aircraft are listed below:

1. Pneumatic boots

2. Electro-impulse (EIDI)

3. Piezoelectric devices

4. Vibratory devices

In all of these mechanical systems, the mechanics of deicing a surface can be divided into two distinct phases: breaking the adhesive bond and shedding the ice. At times, the ice will also crack from bending stresses. However,

1

research has shown that breaking the adhesive bond by peeling or shear forces is the dominant effect. Aerodynamic forces or inertia forces acting on the ice cause shedding.

Recent research work at Ohio State University measured the pressure distribution acting on simulated ice shapes attached to the leading edge of an airfoil.[1] Additional analytical research work is being done at The University of Akron.[2] From these research projects, pressure distributions can be used to determine typical aerodynamic forces acting on the impact ice of wing surfaces. Ice on rotating surface will shed by inertia or G-forces, which are generally much greater than aerodynamic forces.

Because of all of these variables, a basic understanding of the mechanics of adhesion and fracture of ice is needed in order to effectively design deicing systems. A more effective mechanical deicing system would improve the safety of small fixed-wing aircraft and make rotary wing aircraft more effective in cold climates. Because of the importance of the adhesive bond, research efforts have been concentrated on that problem area. Ice-phobic substances, which reduce the adhesion between ice and the base surface can be used with all systems; however, mechanical systems use ice-phobics most often. Since ice-phobics lose their effectiveness with each accretion, and in the rain deicing systems are usually designed assuming phobics are not present.

Thermal systems are also used to deice aircraft. In thermal systems, the heat from the deicer melts the ice layer next to the airfoil surface which reduces adhesion. Final ice shedding is caused by aerodynamic or G-forces. Various thermal systems are available such as electric resistance heaters, hot bleed air and hot circulated fluid. These systems are usually employed in large aircraft because of their high energy requirements. Measurements of the variation of adhesive shear strength with ice/substrate interface temperature

have been made in this investigation.

2.0 Discussion of Literature

Some of the first work on the adhesion of ice to various surfaces was done by Loughborough and his colleagues (3,4). Two methods were used to measure the shear strength of ice: a centrifugal method and special torsional apparatus. The shear strength of refrigerated ice was found to reach 250 psi. Adhesion of artificial ice to metals and polymers was also studied. Adhesive shear strengths varied from 220 psi (aluminum) to 124 psi (copper). Values to various polymers varied from 150 psi to 170 psi. In Reference (4) the work of adhesion was studied.

J. L. Laforte, C. L. Phan, J. Druez and colleagues at the Universite' du Quebec a Chicoutimi have studied the adhesive strength of rime and glaze impact ice on aluminum electrical power conductors cables (5,6,7). In this work, wind velocities were varied from 4 m/sec (9 mph) to 23 m/sec (51 mph). A 20 μm drop size with a 2.8 g/m^3 liquid water content was specified for most studies. Surface roughness was varied from 1 to 19 μm (40 to 750 μ in). The adhesive shear strength was shown to vary from 67 KPa (10 psi) to 400 KPa (58 psi), and increased with both velocity and surface roughness (5); the greatest variation occurred with roughness. Ice densities of impact ice varied from 0.91 g/m^3 to 0.84 g/m^3 and decreased with decreasing temperature (-5°C to -22°C). In earlier work (1976) adhesive shear strength on to various substances including polymers, metals and epoxy were measured. Wind velocities of 10 m/sec (22 mph) and 20 m/sec (45 mph) were developed. The mean drop size was 59 μm. The adhesive shear strength increased with wind velocity. Results for hard rime ice and glaze ice were in general similar.

Itagaki and others studied the adhesive strength of ice using a high speed cylindrical aluminum rotor (8, 9). Tip rotor velocities up to 316 mph were

3

obtained. Adhesive shear strength and ice tensile strength were determined simultaneously by measuring the thickness of the ice accretion at fracture. By assuming a uniform ice accretion and centrifugal inertial loading, formulas for both the tensile strength and adhesive shear strength as a function of ice thickness could be derived. Tensile and adhesive shear strength to 2 KPa (0.3 psi) and 110 KPa (16 psi) were determined respectively. These values appear low when compared to those of other investigators. Furthermore, tabulated data in the report does not seem consistent. Possible bending vibration of the test apparatus and aerodynamic forces may have contributed to these difficulties. Measurement made in Reference (9), ice accretion on cylindrical rotors for some icing conditions was shown to vary with length and to reach a maximum value about 2/3 along the radial dimension of the rotor and then, decrease in thickness to the end of the rotor. This thickness variation may also have affected the evaluation of impact ice strength from high speed rotors since basic formula assumes uniform thickness.

Numerous authors have studied the shear strength of artificial and natural ice as well as the adhesion between ice and other materials. Voitkovskii (10) summarizes some of the Russian and European work (through 1960). The shear strength of natural river ice varied from 6 kg/cm^2 (85 psi) to 13 kg/cm^2 (185 psi) and of artificial ice from 9 kg/cm^2 (128 psi) to 56 kg/cm^2 (796 psi). Values are also listed for iron with temperatures very near the melting point of ice (-0.085°C to -1.09°C). As a result, the adhesive strengths are low 0.14-3.0 kg/cm^2 (2-42 psi).

Jellinek (11-13) studied the adhesive and cohesive strength of a snow-ice sandwiched between polished circular 304 SS plates approximately 0.3 cm apart. Shear stresses were developed from torsional loads. The adhesive strength or cohesive strength (if failure occurred in the ice) increased linearly with

decreasing temperature from 0 kg/cm^2 at 0°C to 16.6 kg/cm^2 (236 psi) at -14°C (6.8°F). Below -14°C there was a slight decrease in strength to 26 kg/cm^2 (228 psi) at -34.3°C (-30°F).

Similar tests were run on Polystyrene. The adhesive shear strength also varied linearly from 0 to 0.43 kg/cm^2 (6 psi) at -15°C (5°F). The effect of roughness of 304 SS plates was studied in another investigation (12). Three surfaces were considered: a machined surface, a mat surface finish and a mirror polish (5 to 7 μ in). Mean adhesive shear strengths were 6.1 kg/cm^2 (87 psi), 2.7 kg/cm^2 (38 psi) and 0.68 kg/cm^2 (9.7 psi), respectively, for a snow-ice layer 0.1 to 0.2 cm thick and a cross section of 6.26 cm^2. Thus, surface roughness increased these shear stress by a factor of almost 10. Adhesion of ice frozen from dilute electrolyte solutions was reported in Reference (13).

The ultimate shear strength of naturual (fresh water) ice as a function of temperature was reported by Kozitsokii (14). Values reached 17 kg/cm^2 (241 psi) at -14°C (7°F) which is similar to results obtained by Jellinek (11).

Tensile properties of artificial ice were thoroughly studied by Hawkes and Mellor.[15] Strain rates were varied from 10^{-6} in/in/sec to 1 in/in/sec. Both tensile and compressive ultimate strains decreased with increasing strain rate. However stresses increased with increasing strain rates. The tensile strength increased approximately 20 bars (290 psi) at 10^{-4} in/in/sec; the compressive strength increased to 85 bars (1232 psi) at 10^{-2} in/in/sec. The initial Young's Modulus in tension increased from 8 x 10^5 psi at 10^{-6} in/in/sec to almost 1 x 10^6 psi at 10^{-3} in/in/sec. The compressive Young's Modulus is approximately constant with strain rate with a value of 1.4 x 10^6 psi. Voitkovskii discusses the effect of static versus dynamic methods of measuring Young's Modulus on ice. Using dynamic methods typical values of

artificial ice varied from 8.8 to 9.8 x 10^3 kg/cm^2 (1.15 to 1.39 x 10^6 psi).
However, for static values, Young's Modulus varied from 33 to 65 x 10^3 kg/cm^2
(470,000 psi to 920,000 psi). Voitkovskii discusses in detail the effect of
creep and, therefore, the magnitude of the applied load on Young's modulus.
Similar conclusions can be made using data presented by Glen. (16).

No data could be found on the tensile or compressive properties of impact
ices. Comparison between some of the shear adhesives properties discussed
above will be made with data obtained from this investigation.

3.0 Data Acquisition

Data used in this report was gathered during a series of test conducted
inside NASA-Lewis Icing Research Tunnel (IRT) facilities using two test
apparatus as described below. Inherent with icing research there is a large
scatter of data, and only average statistical values are mentioned in this
report.

3.1 Test Facilities

The shear test apparatus was originally developed by NASA LRC and was
modified for some of these studies at The University of Akron. Peel force
measurements were made on equipment designed and constructed by The University
of Akron. Development of equipment for evaluating tensile properties of
impact ices is in progress. All testing was conducted in the Icing Research
Tunnel (IRT) at Lewis Research Center, Cleveland, Ohio.

The IRT is a closed loop low speed refrigerated wind tunnel. Its test
section is 1.83 m (6 ft) high and 2.74 m (9 ft) wide. The airspeed in the test
section can be varied from 30 (20 mi/hr) to 480 km/hr (300 mi/h), and the
total temperature can be varied from above 0°C (20 F) down to about -30 °C
(-22°F). According to the present calibration, the icing cloud issuing from 77

air atomizing nozzles can produce a drop size range of from below 10 to about 40 microns (volume median diameter, DVM). The liquid water content (LWC) in the test section can be varied from about 0.3 to 3.0 g/m^3. Not all combinations of DVM and LWC are possible at every airspeed. The DVM and LWC are set according to the present calibration by adjusting the air and water pressures to the spray nozzles. For details about the spray cloud calibration and a discussion of possible error sources, refer to Reference 17. These results indicate that the data reported herein should be free of any significant error.

3.2 Shear Strength Study

Figures 4 and 5 show a photograph and schematic diagram, respectively, of the test apparatus used to determine the adhesive shear strength of impact ices. As shown, the equipment has two main sections: (1) the ice forming section where impact ices are accreted on the test specimens and (2) the test section where the adhesive shear force is measured. Instrumentation of the test section is above the IRT; samples are placed in a holder in the wind tunnel for measurement. The test specimen consists of a thin outer cylinder with a window and end flanges and a hollow inner cylinder.

The inner cylinders of the shear test specimens were fabricated from 304 stainless steel, aluminum and neoprene. The roughness of the metal specimens is 10 to 30 rms micro inches. Prior to each test the metal inner cylinders were dipped in acetone and allowed to dry. The specimens were assembled with metal tongs so that the surfaces were free of grease. Neoprene surfaces were cleaned with alcohol. Inner cylinders were also assembled in the same order. The objectives of this procedure was an attempt to reduce data scatter. The fit between the two cylinders is a sliding fit so that it will slide freely without vibration. Five of the cylinder pairs are stacked (Figure 4-b) on top

of each other on a common shaft which is mounted vertically in the IRT. The assembly is usually rotated in the wind tunnel at a rate of approximately 20 rpm. When the stack is rotated, an almost uniform coating of ice is deposited on to the cylinders. In a few tests the window was aligned up stream and the stack not rotated. When stationary, ice formed over the window and adjacent area only. Two types of windows were used (Figure 6): a square (3 x 2.7 cm) window and a rectangular window (3 x 6.5 cm).

Time of exposure to the ice cloud was varied so that the thickness of ice deposit was approximately 1/4" to 3/8" thick. It was found that if the ice were too thin, cohesive failure would occur in the window section. As expected, this type of failure occured more often with rime ice than with glaze ice. Furthermore, the rime ice accreted with small water drops (15 μm) appeared to be weaker than that developed with larger drops (20 -27 μm). On the other hand, if the ice were too thick, the stack assembly could not be taken apart without significant force which often disturbed the adhesive bond between the inner cylinder and ice. Thus, by trial and error it was found that the optimum thickness for these tests was about 1/4" for glaze ice and about 3/8" for rime ice.

One other aspect about testing rime ice should be pointed out. Bumps and depression in the surface of the specimen affected the shape of the ice deposit. Thus, the lip at the window edge of the outer cylinder could be easily distinguished in a 3/8" ice deposit even though the lip was filed to a sharp edge. This problem was worse with small drops (15 μm) at low temperatures (-8°F). This weakness in rime ice often leads to a cohesive failure along the window edges rather than an adhesive failure on the surface of the inner cylinder. None of these cohesive failure data were used in this report.

Figure 7 shows a thermocouple which is embedded in the center of the inner cylinder wall near the center of the rectangular window. This thermocouple was used to measure cylinder temperature as the specimen was being heated with a cartridge heater. A finite element transient heat conduction calculation was made using NASTAN which accounted for the ice layer, stainless steel housing and inner metal cylinder. It was determined from this analysis that the difference in temperature between the interface and point of measurement was less than about 1°F. When the heater was turned on the temperature on the cylinder rose slowly. From 5 to 10 minutes was needed to reach a predetermined cylinder temperature. The instant a predetermined temperature is attained, the hydraulic cylinder is actuated to shear the specimen. In this manner shear stress as a function of tempertaure was determined. A typical shear test data is shown in Figure 8.

Similar shear tests were conducted previously using various ice phobics on the target cylinder surface. Comparison of data (with similar test conditions) obtained with this test with the previous test, showed that the shear stress measured in the previous test were found to be a factor of 2 to 3 too low. This difference could be explained by the fact that the shearing of the accreted ice from the substrate material happens almost instantaneously (as can be seen in [figure 8), which is almost an impulsive force. The previous study uses a pen chart recorder to record the "impulsive" shear force and the present study uses a storage scope. Due to very high frequency content of an impulsive signal coupled with the inertia of the recording pen, the chart recorder failed to record faithfully the true magnitude of the "impulsive" shear force, thus the difference between the measurements of the two tests.

3.3 Peeling Strength Study

A photograph of the impact ice peeling apparatus is shown on Figure 9

and a schematic diagram on Figure 10. As seen on these figures there are six symmetrically positioned window slots (1" x 6") in the sides of the 16" diameter aluminum drum. Thin rectangular strips (3/4" x 6") of different materials were held flush with the surface of the cylinder with small steel backing plates. The cylinder could be either rotated or held in a fixed position with a specimen up stream in order to build up an ice coating. Specimen strips are peeled from the ice with a thin braided stainless steel wire through a load cell to measure the peeling force. The pulling speed is monitored with a LVDT. Typical output is shown on Figure 11.

Three types of specimens were used in this test: aluminum, 316 stainless steel 0.003" shim stock and a neoprene faced composite. Most of the data were taken with the stainless steel and neoprene specimens. Forces associated with this mode of failure were much lower than expected. As a result, specimens had to be very flexible to avoid stripping the specimen from the ice. For this reason, thin shim stock 0.003" thick was used. However, these specimen had to be mounted carefully to avoid having the specimen pulled out of the window from aerodynamic forces.

The angle of peel can be varied by adjusting the height of the yoke relative to the bottom of the specimen. Peel angles from 20 to 90 degrees could be obtained. The aparatus was designed so that the yoke and point of fracture or peel moved at the same rate and thus, assure peeling at a constant angle. It should be pointed out that peel angles developed from the EIDI or phneumatic boot deicers are less than 2°.

After assembly, metal peel test specimens were cleaned with acetone and neoprene specimens with alcohol. Care was taken to seal the edges of the specimens so that there was no sandwich bond between specimen and the large cylinder.

4.0 Discussion of Results

Experimental results have been divided into four parts: preliminary adhesive shear test results, shear strength as a function of interface temperature, shear strength as a function of velocity and peel test results. Data in the IRT were collected in three separate test series each approximately one week long.

4.1 Parametric Study

Parametric experimental studies revealed that the adhesive shear strength of accreted impact ice to be statistically independent of the following:

4.1.1 Tunnel Air Temperature Below 4°C (25°F)

Figure 12 shows a scattered data plot of the variation of shear stress vs. temperature, as can be seen, its dependence on temperature is negligible.

4.1.2 Thickness of Accreted Ice

Figure 13 shows that shear stress is relatively independent of ice accreted thickness. Thickness of the impact ice was varied from 1/16" to almost 1/2". In cases where there was a clear shear fracture, there was no statistical difference in the adhesive strength.

4.1.3 Metal Substrate

Figure 14 shows the statistical plot of shear stress vs. material substrate. As shown from the plot, the statistical averages of the shear stress is almost equal for two identical icing conditions.

4.1.4 Other Parameters

Figures 15, 16, and 17 show very negligible variation of the adhesive shear stress to (a) different window shape (Rectangular/Square), (b) the

11

testing condition whether cloud off or cloud on and (c) the ice accretion shape whether the stack of specimens (Fig. 4b) is rotated (uniform) or un-rotated (non-uniform) during accretion of impact ice, respectively.

In conducting the part (b) experiment above, a special specimen that could not rotate, which was fixed directly to the platform (Figure 7) was developed. The shear stress was then measured while the icing cloud and the ice was still accreting (i.e., the air speed was on). As mentioned above, no appreciable difference in adhesive shear strength was noted.

To test the effect of surface roughness a number of specimens were sand blasted. In aluminum samples, the roughness was increased from 10 - 30 μin rms to 40 -50 μin rms. The adhesive force for a roughness of 10-30 μ in r.ms. varies between 40-60 psi but for the 40-50 μ in r.ms., roughness, the test apparatus could not induce adhesive failure; the maximum force reached was 160 lbs (about 114 psi). These data and the resuults in the literature suggest that roughness is a major parameter affecting the adhesive strength.

Three parameters examined in this study had correlative effects with the adhesive shear strength: (1) wind velocity (2) drop size and (3) ice surface temperature. Roughness was not varied systematically in these studies. It was held constant; the same target cylinders were used for many tests.

There was significant effort made to eliminate variables in the testing conducted to measure the adhesive shear strength. However, there is significant data scatter in all shear test results. Mean values and standard deviations are shown in the figures.

4.2 Shear Strength versus Ice-Substrate Interface Temperature.

Figure 13 shows a scatter plot of all data collected from this experimental series. As can be seen, there appears to be a strong correlation

between the ice-substrate interface temperature and the adhesive shear strength. At an interface temperature above 25°F, the shear strength, on the average, tends to decrease and approaches zero at the melting point temperature of 32°F. Also shown superimposed to it is the statistical plot of the data. In this case, only statistical mean shear strength at selected interface temperatures with adequate data sample for a statistical mean analysis are shown. There is a the gap of missing data between temperatures of 2° and 8°F, nevertheless there appears to be a sharp decrease of the adhesive shear strength at temperature above 25° F. The average data ($\pm$ 2σ standard deviation) is $\pm$ 42% of the average reading. This scatter is much more than similar data for conventional structural materials. This scatter is believed to be inherent, because tunnel conditions are quite repeatable and the test specimens were carefully cleaned and prepared in the same manner.

4.3 Adhesive Shear Strength versus Wind Velocity

Figures 19 and 20 show both a scatter plot and statistical averages of data points obtained from these test series. Figure 19 shows the variation of adhesive shear strength with wind velocity for hard rime and glaze ice deposits (12 -18°F tunnel temperature). As can be seen in Figure 19, for hard rime-glaze ice, the adhesive shear strength appears to increase slightly as the wind velocity and drop size increases which is confirmed by the statistical curve also.

However, for powdery rime ice (-8°F to 3°F) in Figure 15, there appears to be no discernable trend at all (also confirmed statistically). In the majority of the test samples with these particular conditions, the ice deposits at the window shattered during the shearing test, and because of this, very few samples were left that gave reliable test values. Therefore for this particular condition the statistical conclusions is not reliable due to limited statistical points.

13

4.4 Adhesive Shear Strength versus Droplet Momentum

Figure 21 shows a statistical plot of shear strength versus the droplet momentum for hard rime-glaze ice conditions. As can be seen, the strength increased slightly with increasing droplet momentum.

4.5 Peeling Strength Test

Figure 22 shows the variation of the peeling stress (Force/unit width) with the different substrate materials. As can be seen, the peeling stress for neoprene tends to be higher than for metal strips. However, both values are low and vary between 2 and 4.8 lb/in.

The lowest peel angle obtained with the apparatus was approximately 20 degrees. There was no significant increase in peel strength from 20 to 90 degrees. A few experiments were performed manually at 0 angle of peel. This test is equivalent to the shear strength obtained from the shear test apparatus. For this case, a very large full adhesive shear strength was obtained. The peel strength between 0 and 20 degrees could not be investigated with the current apparatus. Further testing is needed to examine this region because pneumatic and EIDI deicers operate with less than a 2° peel angle.

4.6 Ice Bending Fracture Test

Deicing using either pneumatic boots or electro-mechanical impact systems cause ice to fail in three modes: shear, peeling, and tension. Tension failures are caused by bending of the impact ice. As a result, tensile bending stress failures must be taken into account in the mathematical modeling of deicing systems.

Preliminary tests were conducted to determine the tensile cracking characteristics of refrigerator ice coated on metal specimens. In this investigation, specimens were cracked using a STRESSCOAT strain indicator, shown

on Figure 27. In order to visually record the result food dye was applied to the cracked ice.

Ice was bult up on a specimen by first freezing the aluminum beam and spraying water onto the beam until a thickness of approximately 0-16 cm (1/16") was obtained. Specimens were cracked at three temperatures: -9° C, -18° C, -29° C (15° F, 0° F, and -20° F). Fracture of the first few specimens was characterized by a tensile failure in the area of high strain followed by a shear failure at the metal-ice interface and lifting of the ice layer. In order to prevent this type of shear failure the aluminum beam specimens were sandblasted to roughen the surface and increase the shear strength at the interface. This precaution reduced but did not eliminate shear failure at the interface. Typical specimen which failed in tension is shown in Figure 7.

5.0 Finite Element Study

The long range objective of this effort is to develop analytical procedures to predict deicing of aerodynamic surfaces. Physical properties of impact ices are required as input to any analytical method. Because of the complex shapes of aerodynamic and ice sufaces, it is planned to formulate analytical procedure using Finite Element Analysis, (FEA). Therefore mechanical deicers seem to debonds the ice because of stress concentrations. The main complexity is the accurate prediction of local stress concentrations. A resort to fracture mechanics approaches may be needed.

5.1 Shear Test Modeling

A finite element study of the shear test specimens was conducted in order to access the magnitude of stress concentration effects on the two types of test specimens. Intuitively, it was felt that stress concentration effects associated with the rectangular window specimen would be less than those of the

15

square window specimen. As a result, finite element models were developed for each type of specimen for both a relative and absolute evaluation of these stress concentrations.

Two sets of boundary conditions were specified for each specimen type. First it was assumed that the ice was fixed to all edges of the window in the outer cylinder. In the second case, it was assumed that the ice accretion was fixed along the two sides of the rectangular windows and to the two sides and bottom of the square window. The second set of boundary conditions was believed to be more realistic and the results of these two analyses are presented on Figures 23 through 26. For the square window it is assumed that tensile failure will occur between the top and bottom flanges and outer cylinder. As a result, there is no support along either the top or bottom edge of the ice accretion on the rectangular window.

Figures 23 and 24 show the normal and shear stress distributions, respectively, for the square windows. As can be seen from these results, there are significant shear stress concentrations at the boundary of the accreted impact ice and outer cylinder. The norml and shear stress distributions for the rectangular window are plotted on Figures 25 and 26, respectively. As seen from these results stress concentration effects appear to be even larger than those for the square window. Thus, this modification did not lead to a more uniform shear stress between the inner cylinder and impact ice. Test results indicate that the average shear stress from the two types of specimens were not statistically different.

In conclusion, shear stress concentrations based on the average shear stress of 4.3 and 5.9 were determined from the finite element study. This effect probably reduced the measured average adhesive stress approximately by a factor of 2.

5.2 Bending Fracture Modeling

To model the Bending Fracture Test, it was decided to use the ADINA program since it has a concrete fracture model that can be used to model the fracture of brittle materials such as ice.

In order to model the beam bend test specimen described above, the tension strength of ice had to be specified. A value of $690 \times 10^3 N/m^2$ (100 psi) was chosen and based on the work of Glen [3]. The finite element model developed of the aluminum beam-ice composite is shown on Figure 2.7. There was a great deal of difficulty in obtaining convergence of the fracture mode. Load steps were reduced from 27.6×10^2 to 62 N/m^2 (0.4 lbs to 0.0089 lbs) before prediction of fracture of the elements stabilized. The model predicted the interval of cracking approximately 1.3 cm (0.5") along the length of the beam which agrees reasonably well with observed fracture.

6.0 Comparison of Results with Other Investigators

Adhesive shear strength of impact ice obtained by Laforte et al (3-5) was 58 psi at 51 mph with a surface roughness of 750 μin. The mean value obtained in this study was 51 psi (Figure 14). Furthermore, adhesive strength by Leforte increased with wind velocity with a variation from 9 mph to 51 mph. In this study, the velocity was varied from 50 to 200 mph; a similar trend was observed; the shear strength increased with wind velocity. It was also found that adhesion increased with wind velocity as well as with the mass of the drop. There are no data in the known literature to compare with the high velocity data obtained in this investigation.

Values of adhesive shear strength reached about 250 psi in artificial ice. Higher values were usually obtained in tests described in the literature in which stress concentrations are kept at a minimum. Peak values of approximately 110 psi were obtained in this study. When the effects of stress

concentration are considered, these results seem reasonable.

The effect of surface roughness on the adhesive shear strength is quite significant in this study as well as the literature. Many studies in the open literature do not quantify this effect. Additional controlled studies on roughness are needed.

7.0 Conclusions

Data from two test apparatus, an adhesive shear test rig and a peel test rig, were obtained in the Icing Research Tunnel at the NASA Lewis Research Center.

This series of tests have provided some additional data on the mechanical properties of rime and glaze impact ice under controled conditions. Results are in general agreement with those of other investigators.

The maximum adhesive shear strength between impact ice and smooth metal or neoprene surfaces can reach 120 psi. Typical values vary between 40 psi and 80 psi. The adhesive shear strength increases slightly with wind velocity and drop size. A correlation with droplet momentum was developed.

The adhesive shear strength is not affected by interface surface temperature at temperatures below 25°F. Between 25°F and the melting point there is a linear drop in adhesive shear strength.

Many aluminum and steel specimens were tested. The shear strength did not vary with either of these metal surfaces. A few neoprene specimens were also tested. Values of these data which are presented in Appendix A indicate that the adhesive shear strength of impact ices with neoprene is similar to that of the tested metal surfaces.

Results of parametric studies also showed that the adhesive shear strength was not affected by ice thickness, cloud on-cloud off conditions, the material substrate (aluminum or 304 SS) rotation or nonrotation of the

shear specimen or the slope of the window of the shear test specimen.

Adhesive shear strength results showed significant scatter. Ice strength measurements of other investigators also had similar scatter. Fracture characterisitcs of most material shows scatter; but the scatter for ice is much greater. The consequences of the large inherent scatter have not yet been fully determined but it clearly is important for deicers and for ice shape determinations.

Stress concentration effects of 4.3 and 5.9 were calculated using finite element analyses for the square and rectangular windows, respectively. This effect has probably reduced the measured adhesive shear strength by a factor of about 2. Stress concentrations of this type will occur with any shear testing. Deicing systems also take advantage of stress concentrations to efficiently debond the ice.

The peel strength of ice between either metal or neoprene surfaces is extremely low and varies between 1 and 5 pounds/inch, at higher than normal peel angles.

ACKNOWLEDGEMENTS

References

1. Bragg, Coirer W.J., "Aerodymic Measurements of an Airfoil with Simulated Glaze Ice", AIAA-86-0484, AIAA 24th Aerospace Sci. Meeting, Reno, Jan. 1986.

2. Potapczuk M.G. and Gerhart P.M. "Progress in Development of a Navier-Stokes Solver for Evaluation of Iced Airfoil Performance", AIAA-85-0410, AIAA 23rd Aerospace Sci. Meeting, Reno Nevada, Jan., 1985.

3. Loughborough, D. L. and Hass, E. G., "Reduction of Adhesion of Ice to De-Icer Surfaces.", Journal of Aeronatutical Sciences, Vol. 13, No. 3, March 1946.

4. Loughborough, D. L, "The Physics of the Mechanical Removal of Ice from Aircraft", Aeronautical Engineering Review, Vol. 11, No. 2, February 1956.

5. Druez, J. Phan, C. L., Laforte, J. L., and Nguyen, D. D., "The Adhesion of Glaze and Rime on Aluminum Electric Conductors", Transactions CSME Vol. 5, No. 4, October 1979, pp. 215-220.

6. Phan, C. L., McComber, P., and Mansianx, A., "Adhesion of Rime and Glaze on Conductors Protected by Various Materials", Transactions CSME, Vol. 4, No. 4, 1976-77, pp. 204-208.

7. Laforte, J. L. Phan, C. L., Felin, B. and Martin, R., "Adhesion of Ice on Aluminum Conductor and Crystal Size in the Surface Layer", CRREL Special Report 83-17, 1983.

8. Itagaki, I., "Mechanical Ice Release Processes: Self Shedding from High Speed Rotors", CRREL Report 83-26, October 1983.

9. ACkley, S. F., Lemieux, G. E., Itagaki, K. and O'Keefe, J., Symposium on Snow and Ice Control Research, Hanover, N. H., May 15-19, 1978.

10. Voitovskii, K. F., "The Mechanical Properties of Ice" Research Report 38, U.S. Army Snow, Ice and Permafrost Research Establishment, Corpos of Engineers, Wilmette, Ill., September 1957.
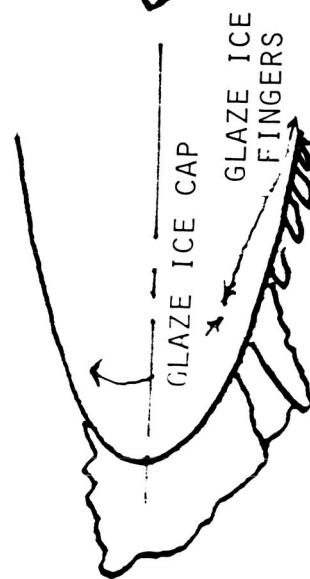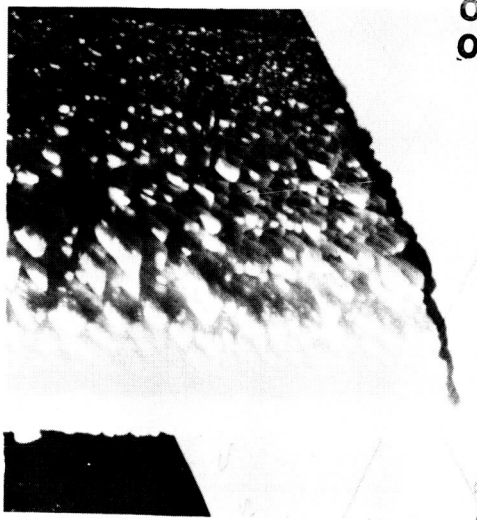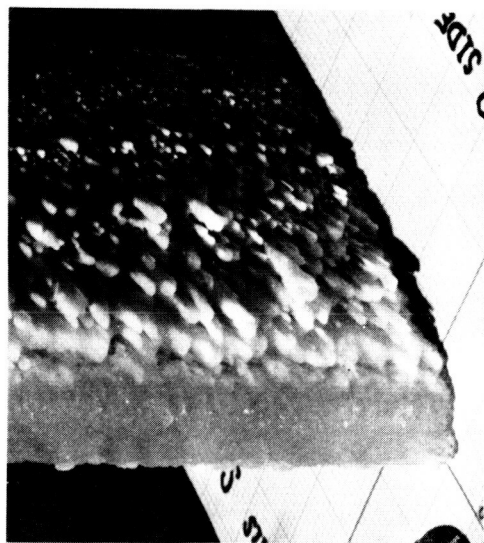
11. Jellinek, H. H. G., "Adhesio of Ice Frozen from Dilute Electrolyte Solutions", CRREL, DA Project IT061102B52A, March 1974.

12. Kozitsokii, I. E. "The Shear Strength of Ice", Metoralogiya i Gidrologiya, No. 3, pp. 103-105, 1978.

13. Hawkes, I. and M. Mellor, "Deformation and Fracture of Ice Under Uniaxial Stress", Journal of Glaciology, Vol. 11, No. 61, 1972, pp. 103-131.

14. Glen, J. W., "The Mechanics of Ice", CRREL, Monograph 11-C2b, December 1975.

14. Glen, J. W., "The Mechanics of Ice", CRREL, Monograph 11-C2b, December
     1975.

15. Olsen, W., D. Takevchi and K. Adams, "Experimental Comparison of Icing
     Cloud Instrucments", NASA JM 83556, Lewish Research Center, Cleveland,
     Ohio, January 1984.

FIGURE 1 TYPICAL IMPACT ICE ACCRETION IN AIRFOIL

0012 Airfoil at 4 degree angle; .53 chord; LWC, 1.3 g/m^3; 8 min. spray; 20 micron drops; 209 km/hr airspeed.

a) Horn-glaze ice at $-8^\circ C$ b) Mixed glaze and rime ice at $-15^\circ C$ c) Rime ice at -26 C

RIME ICE FINGERS

RIME ICE CAP

GLAZE ICE

RIME ICE FINGERS

GLAZE ICE CAP

GLAZE ICE FINGERS

TOTAL -15°C
TEMP.

STREAKS

TOTAL -8°C
TEMP.

LARGE
BUBBLES

TOTAL -2°C
TEMP.

STREAKS

TOTAL -18°C
TEMP.

WHITE
RIME
ICE
OPAQUE

TOTAL -26°C
TEMP.
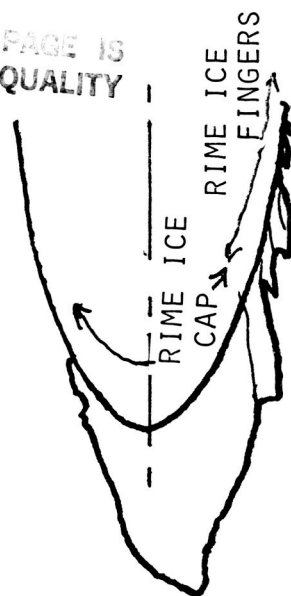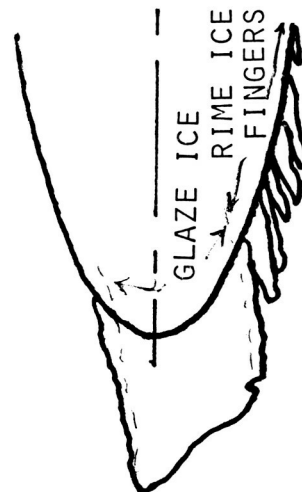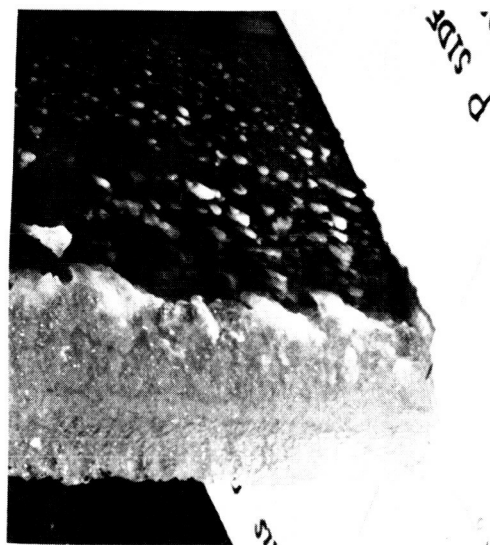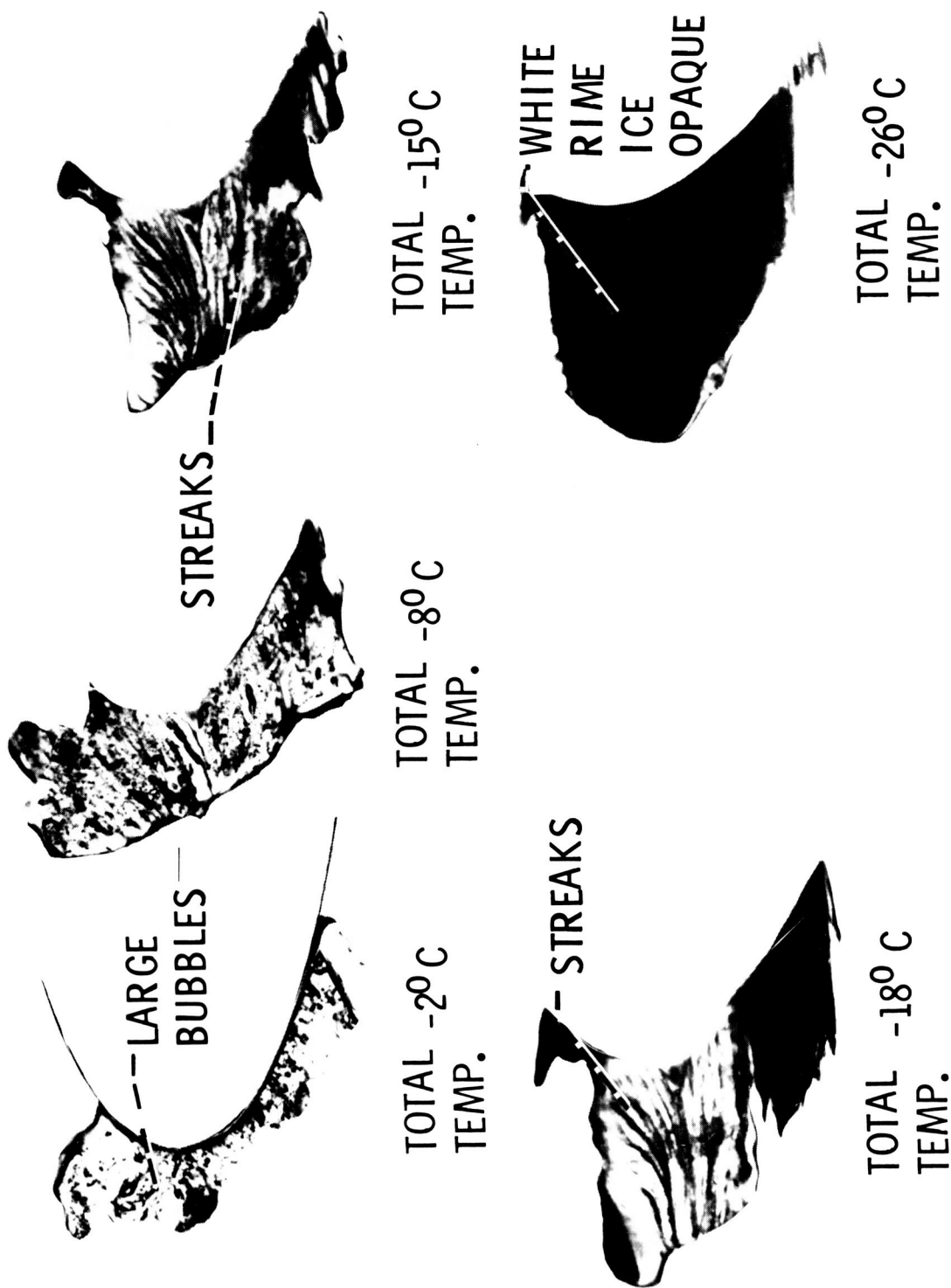
- Effect of temperature on the ice structure. Thin ice samples removed from the airfoil and backlighted; Airspeed, 209 km/hr; LWC, 1.3 g/m³; DVM, 20μm; Time, 8 min; Airfoil, 0.53 m chord 0012 airfoil at 4 deg. angle.

FIGURE 2 BACK LIGHTED PHOTOGRAPH OF IMPACT ICES

3 MINUTE RIME ICE ADDED
$(-26^0 C, 1.7 g/m^3)$

15 MINUTE RIME ICE FORMED
AT $-26^0 C, 1.7 g/m^3$

DYE SPRAYED BY HAND OVER
ENTIRE RIME SURFACE
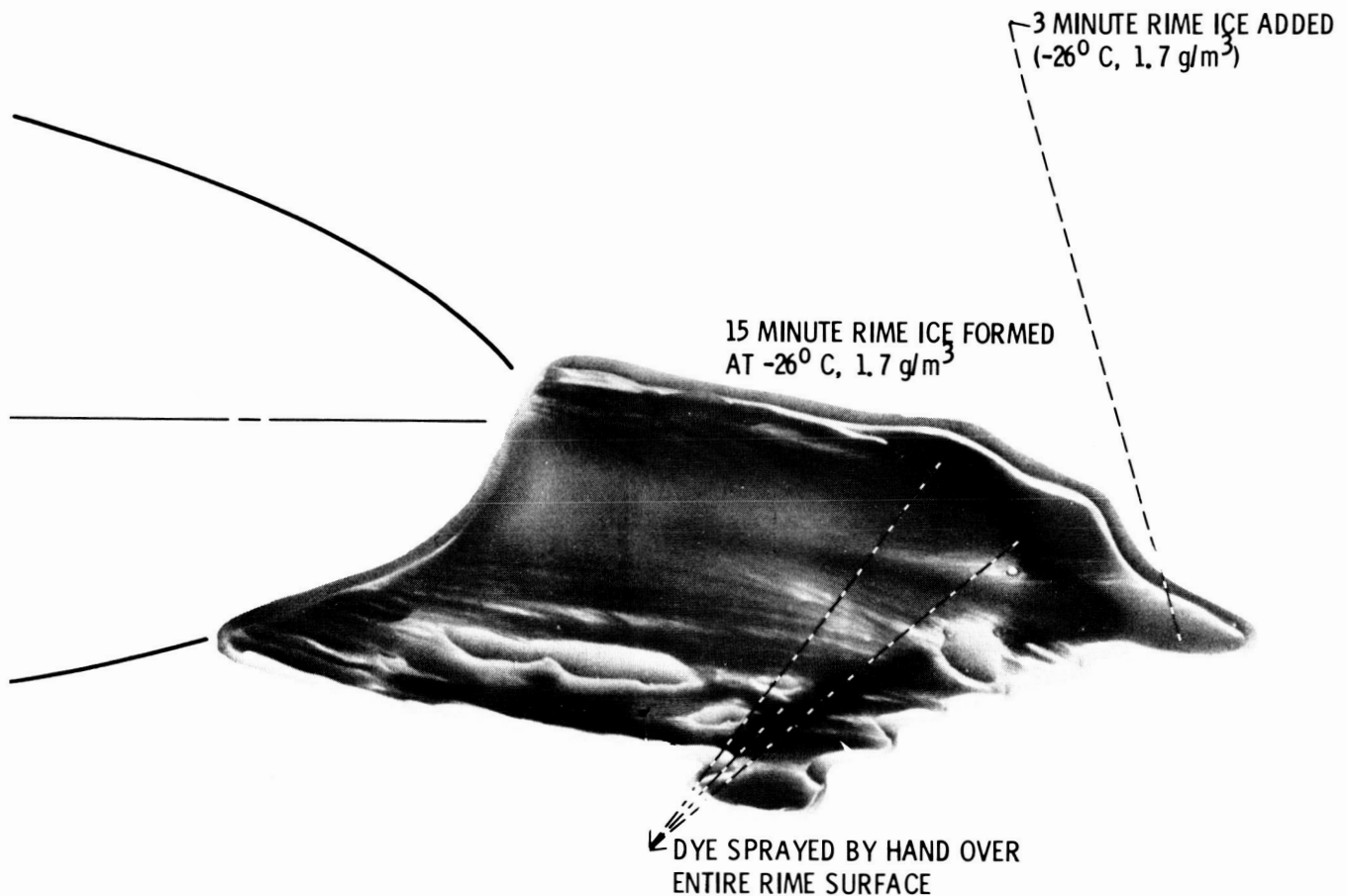
The effect of the ice shape on the droplet catch. Backlighted thin ice sample of a 3 minute rime spray on top of the initial ice shape. For all sprays: DVM, 20µm; airspeed, 209 km/hr.

FIGURE 3 TYPICAL RIME ICE ACCRETION PROFILE
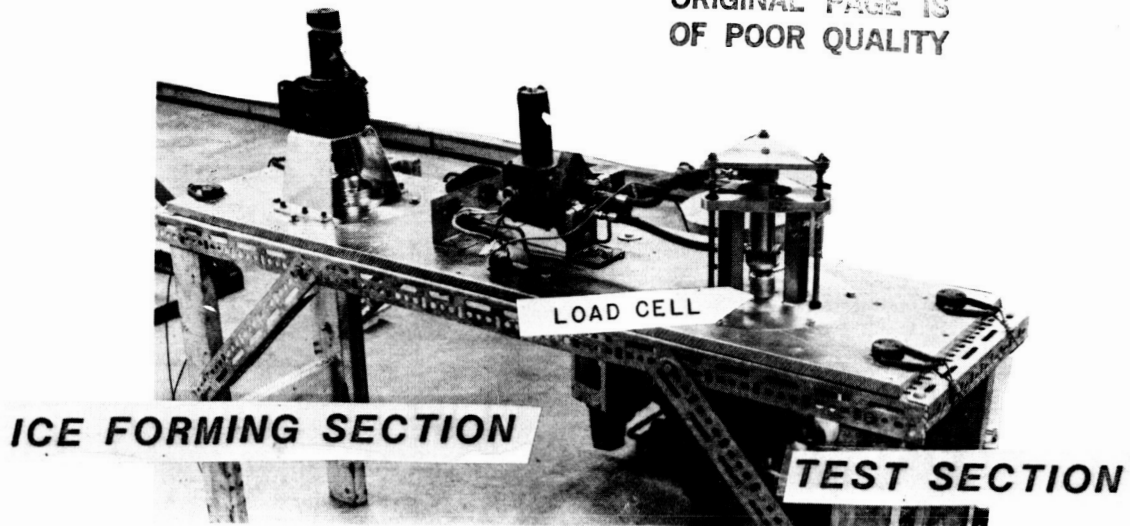
SHEARING TEST APPARATUS
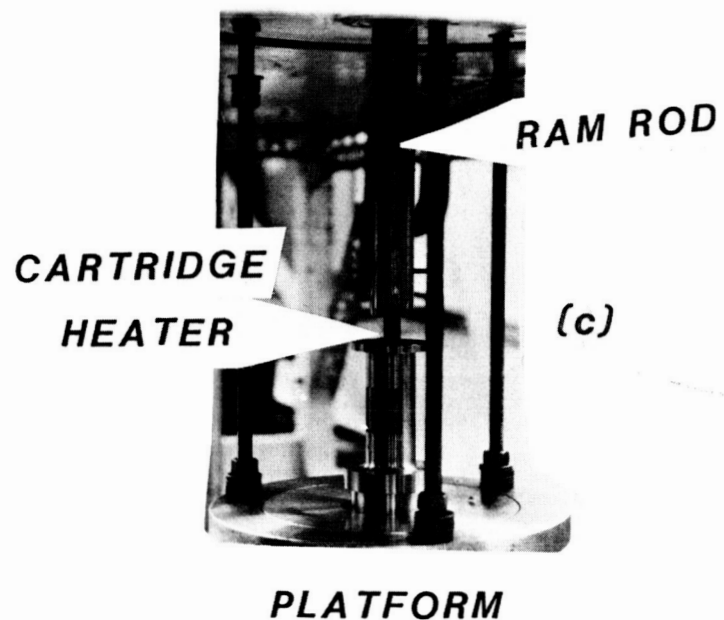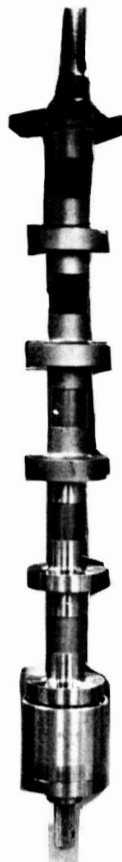
SHEAR TEST SPECIMENS

FIGURE 4 ADHESIVE SHEAR STRENGTH TEST SET UP
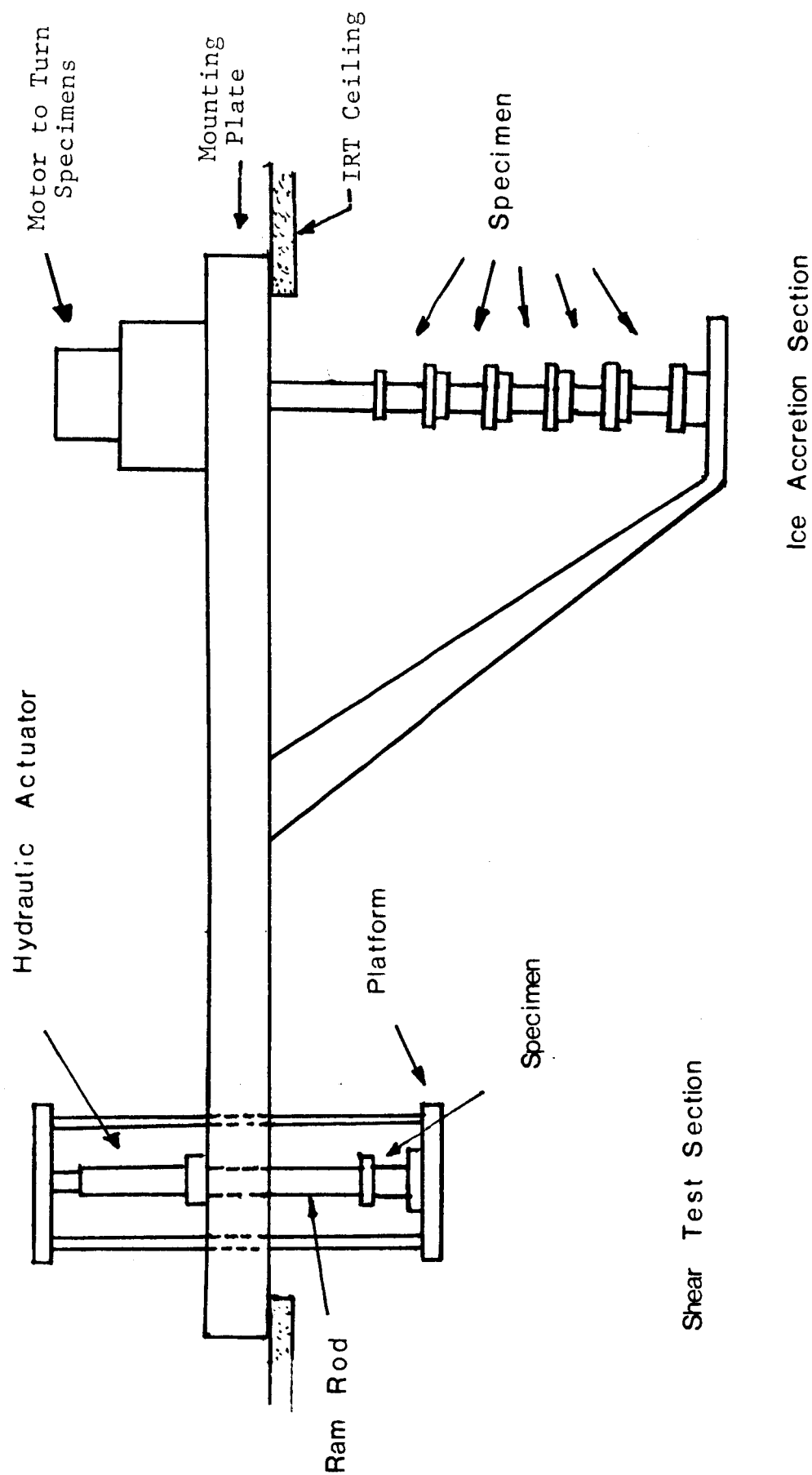
FIGURE 5 SCHEMATIC OF SHEAR TEST SET UP

Motor to Turn Specimens

Mounting Plate

IRT Ceiling

Specimen

Hydraulic Actuator

Platform

Specimen

Ram Rod

Shear Test Section

Ice Accretion Section

Inner Cylinder

Outer Cylinder
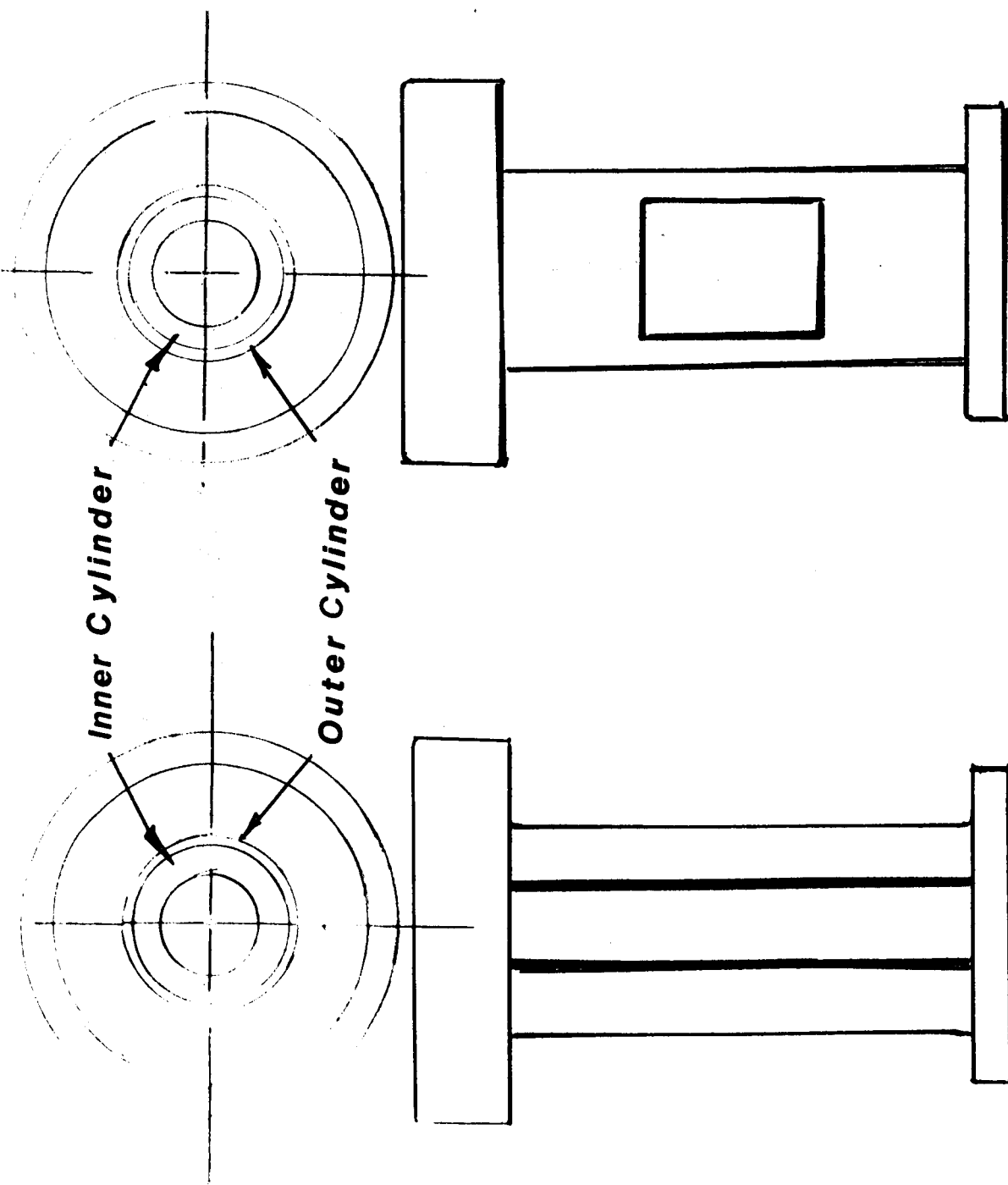
rectangular window   square window

SCHEMATIC OF SHEAR TEST SAMPLE

FIGURE 6

LOAD CELL

BASE PLATE

GUIDING
SLOTS

RAM ROD

CARTRIDGE
HEATER

INNER(HOLLOW)
CYLINDER

THERMO-COUPLE

OUTER
CYLINDER
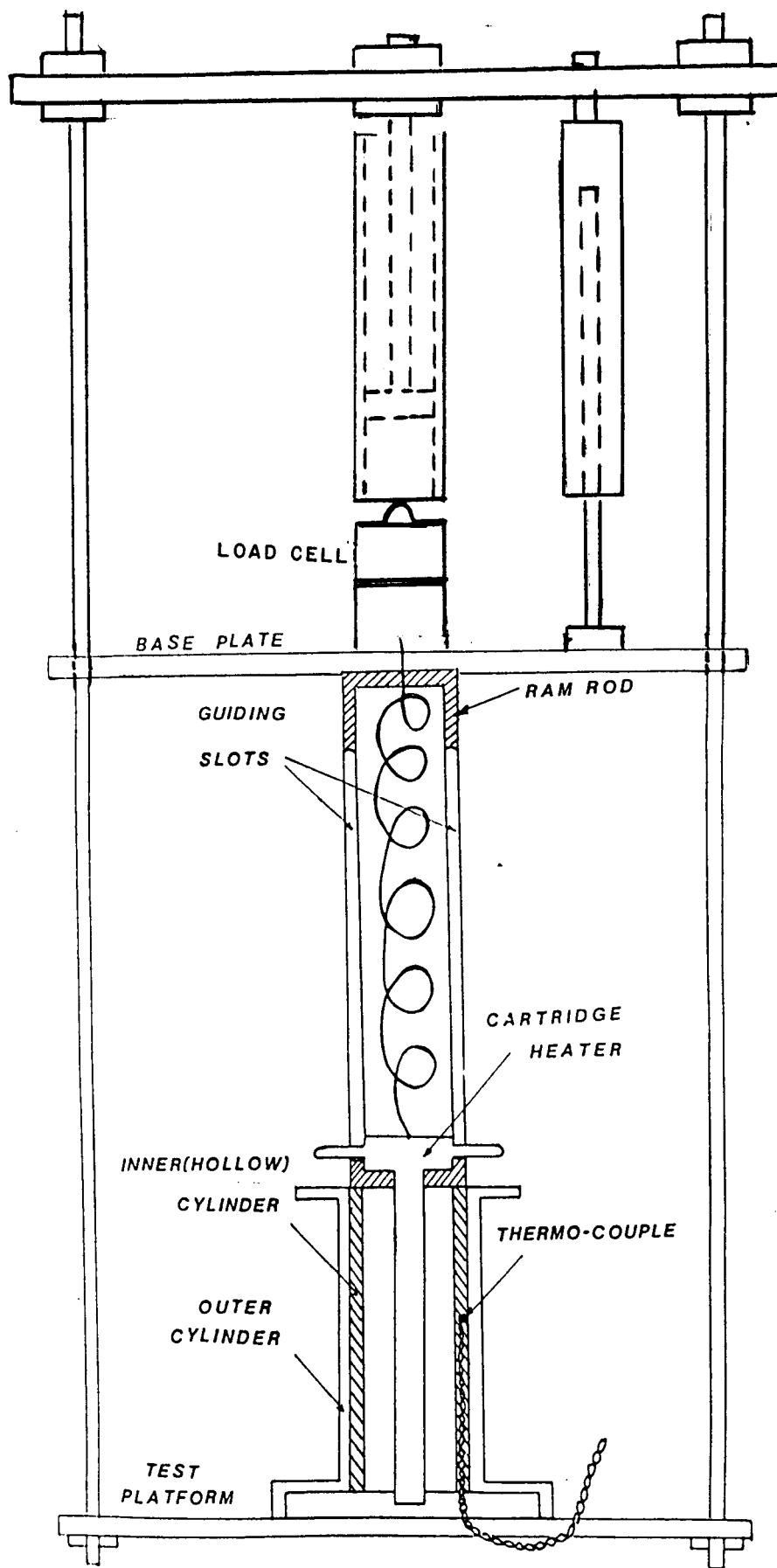
TEST
PLATFORM

SHEAR STRESS TEST SECTION

FIGURE 7 SHEAR VS. INTERFACE
TEMPERATURE TEST SET UP

LOAD CELL

GOOD

LVDT OUTPUT

TYPICAL SHEAR TEST DATA

NO-GOOD
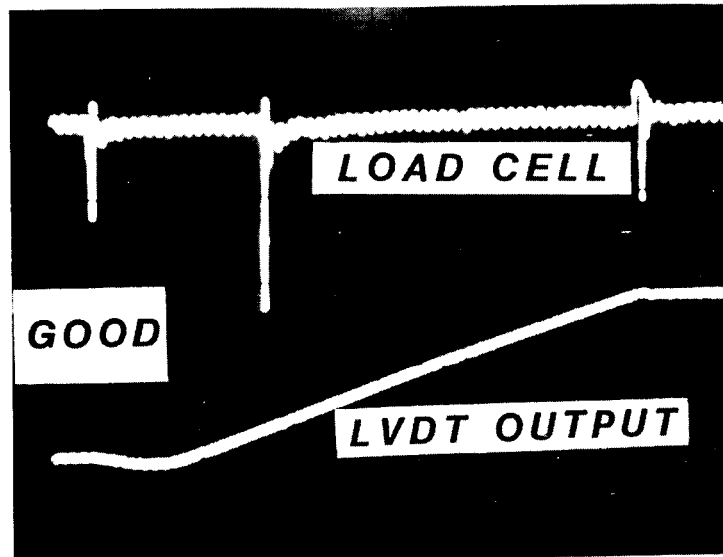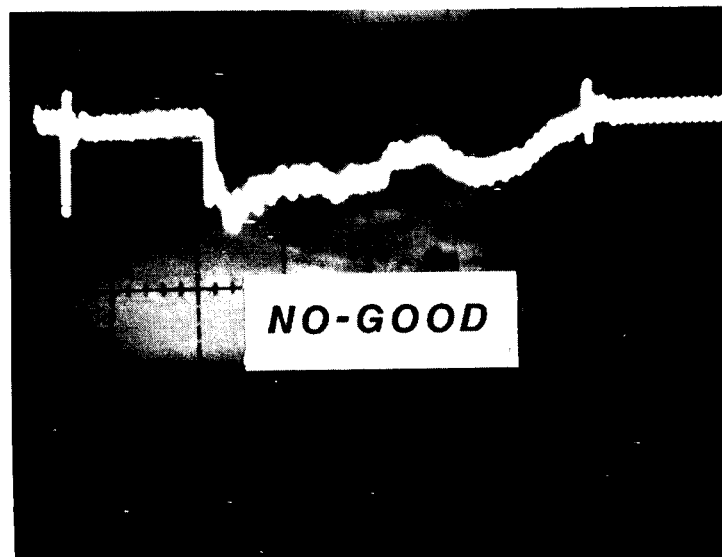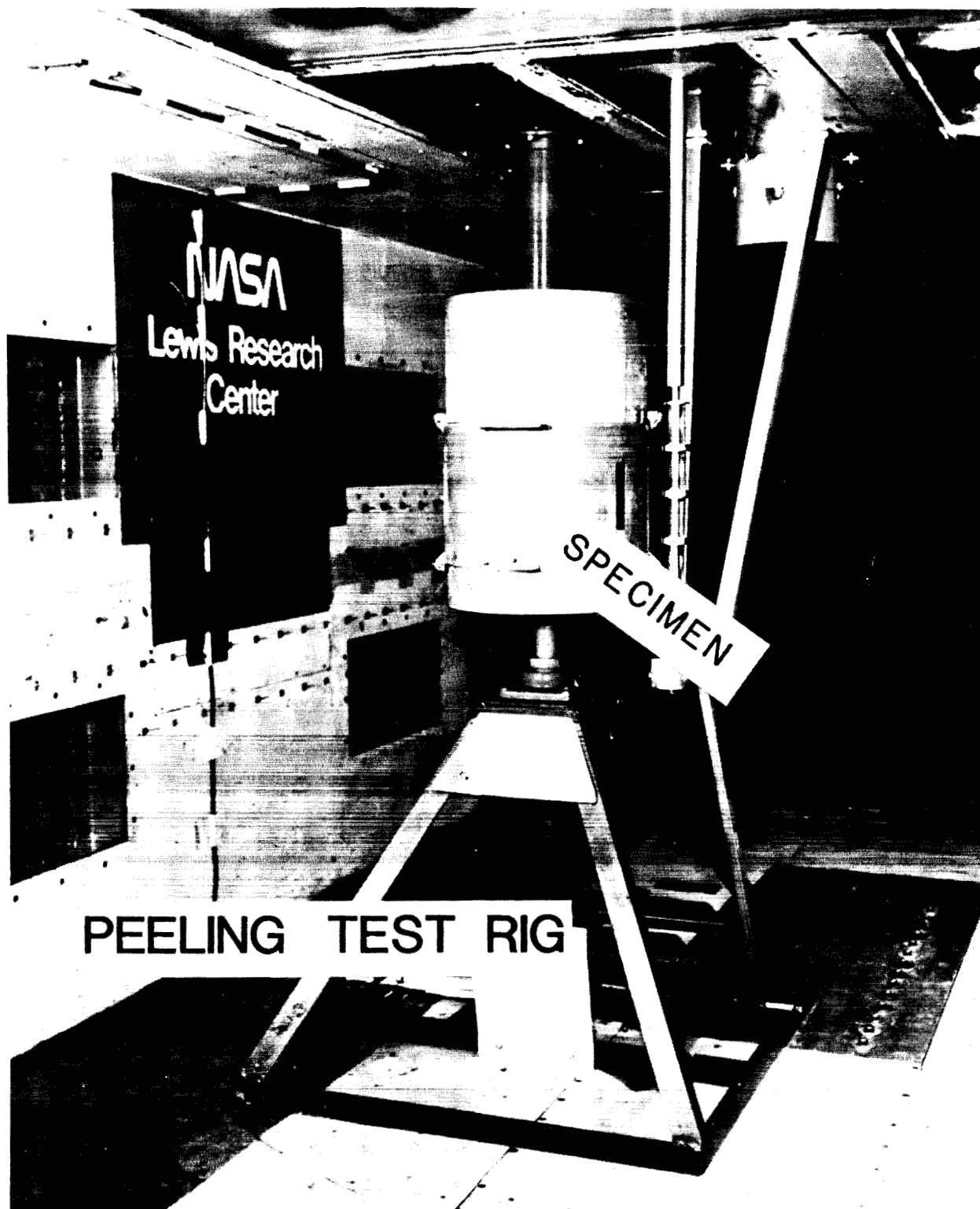
FIGURE 8

FIGURE 9 PEELING TEST APPARATUS
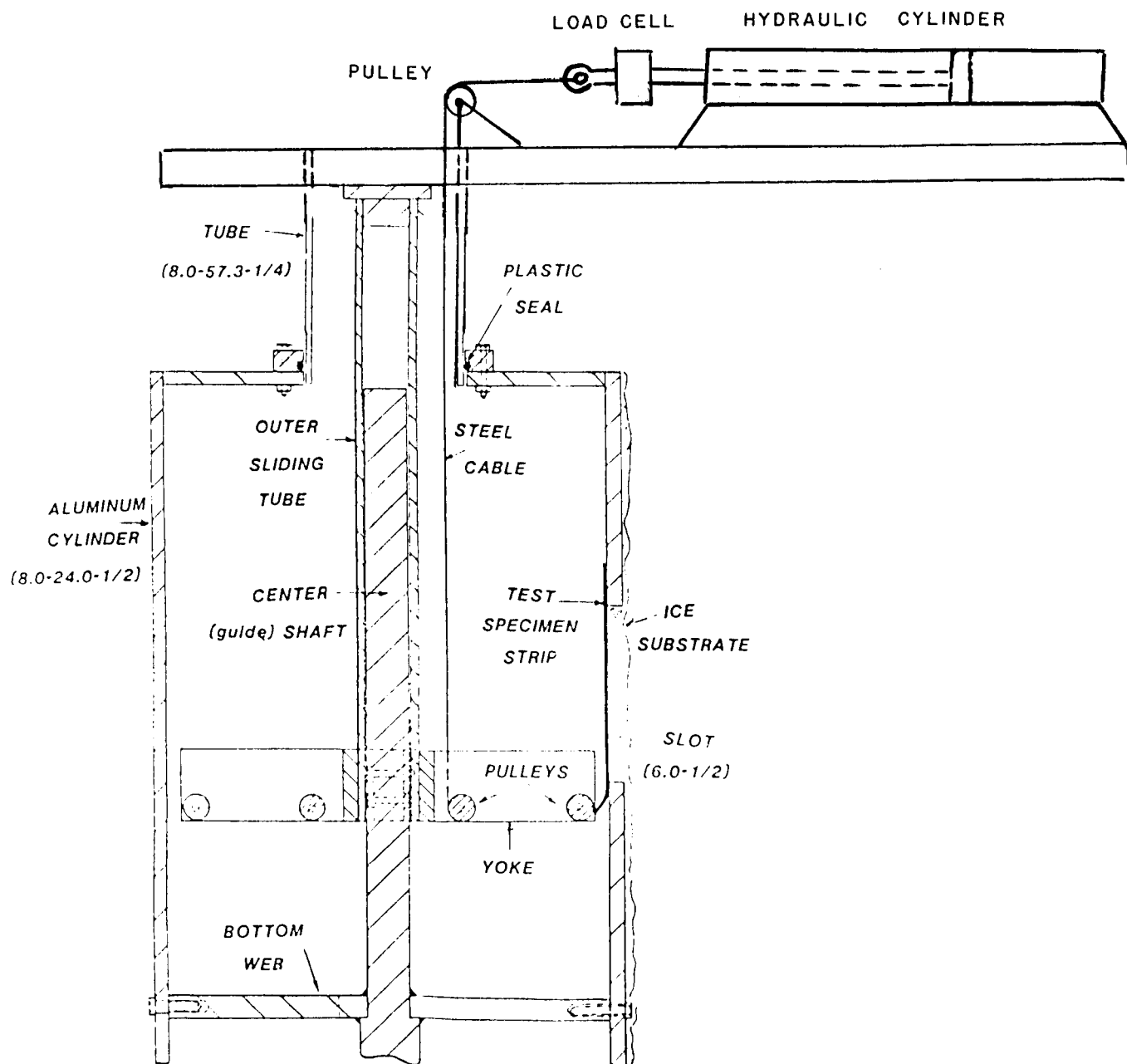
PEELING STRENGTH TEST SECTION

FIGURE 10 SCHEMATIC OF PEELING TEST APPARATUS
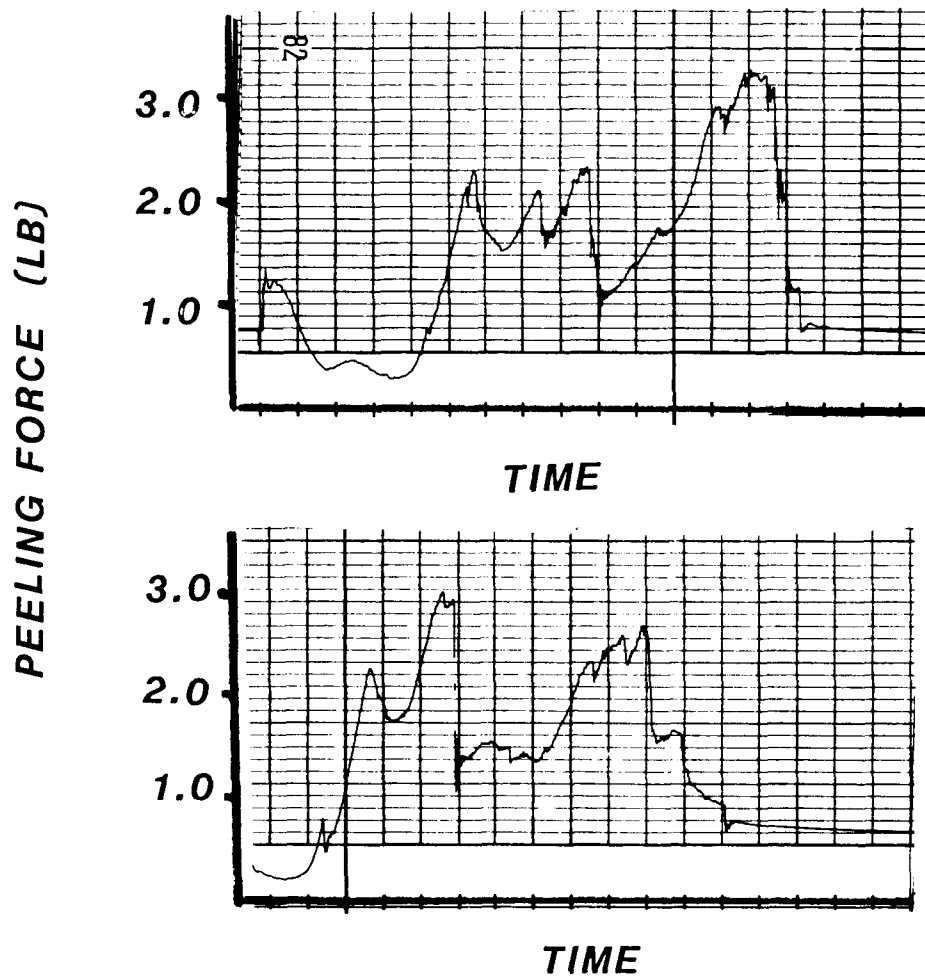
TYPICAL PEELING TEST DATA

FIGURE 11
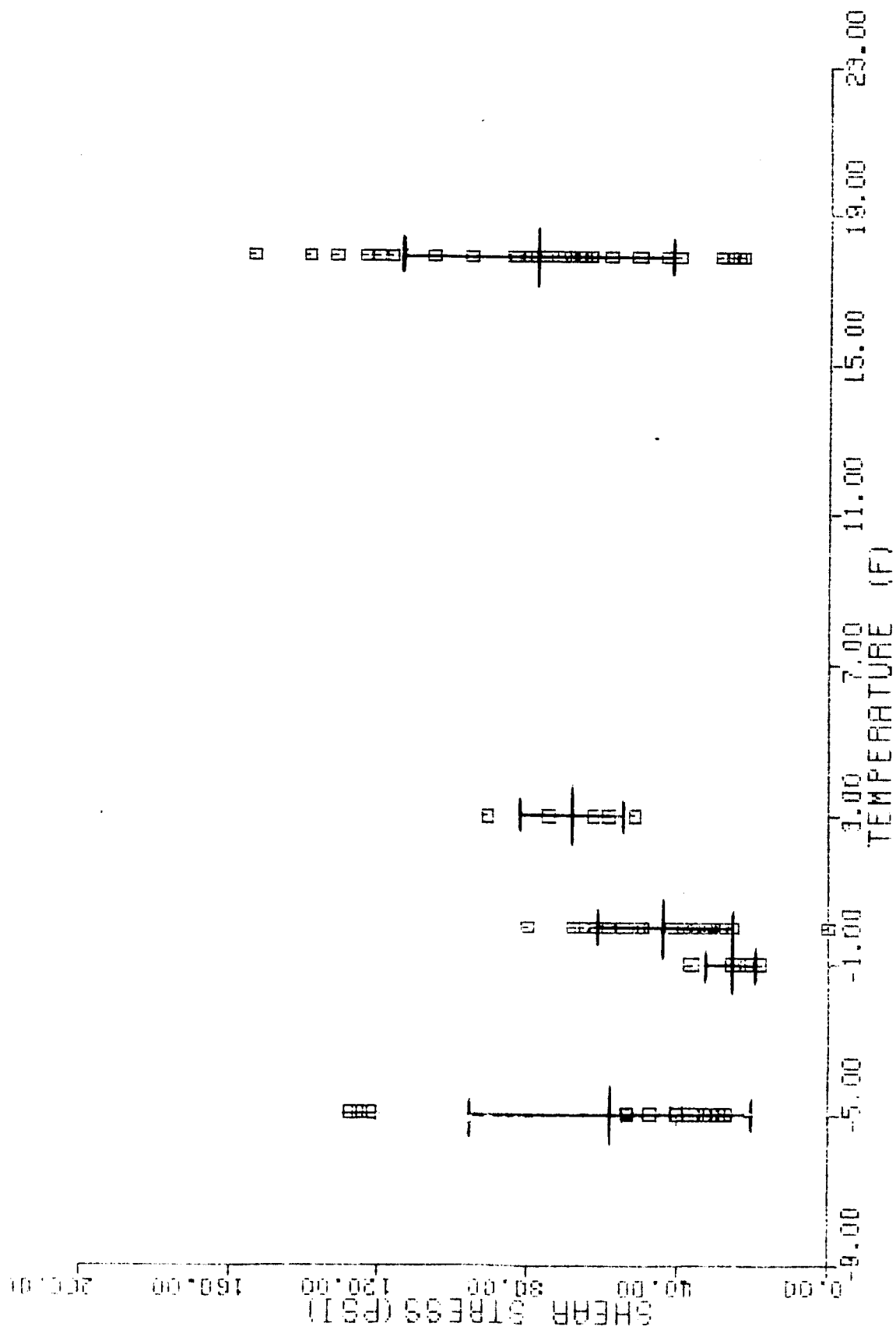
FIG. 12 SHEAR STRESS VS. TEMPERATURE
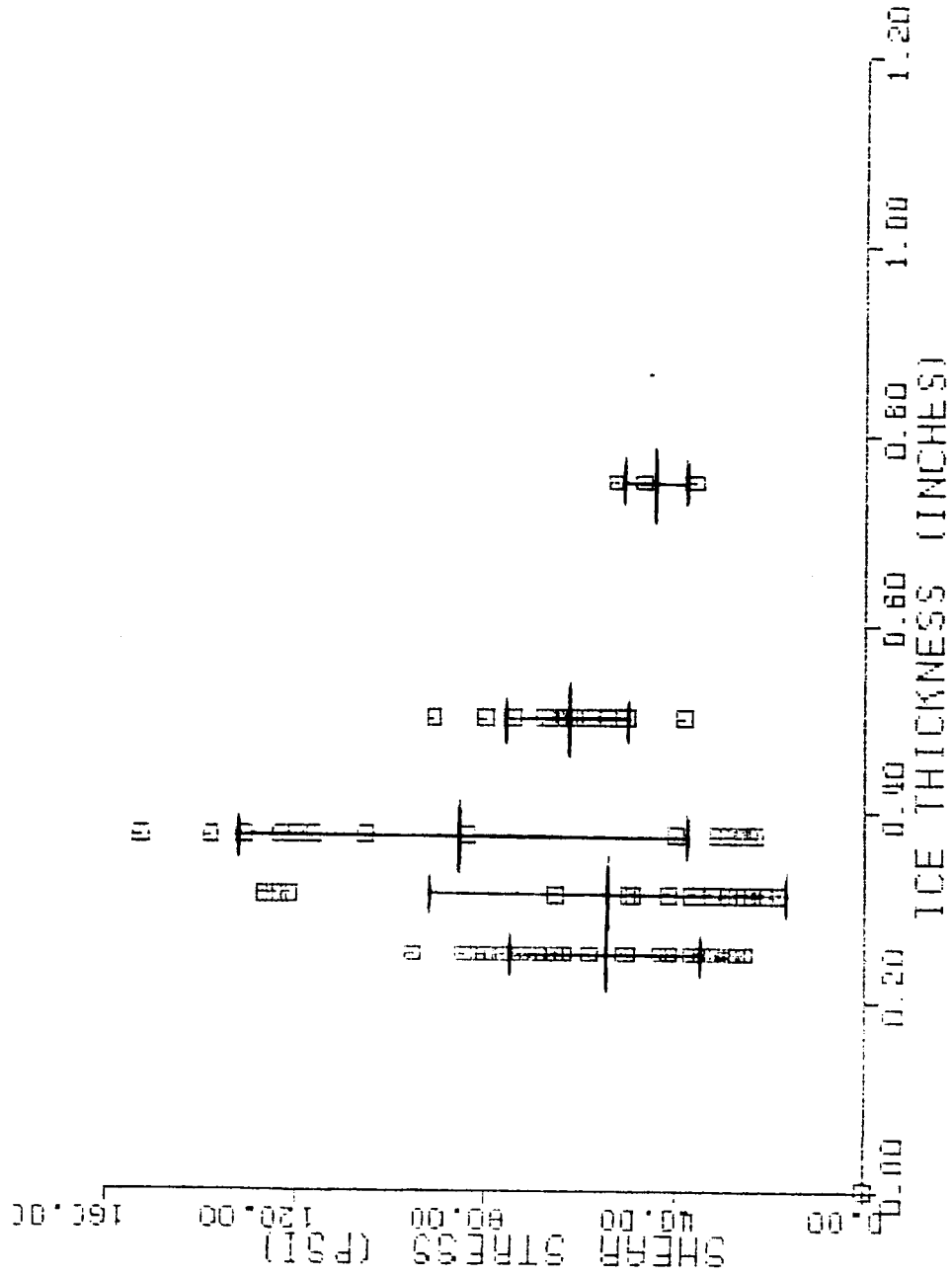
FIG. 13 SHEAR STRESS VS. ICE THICKNESS
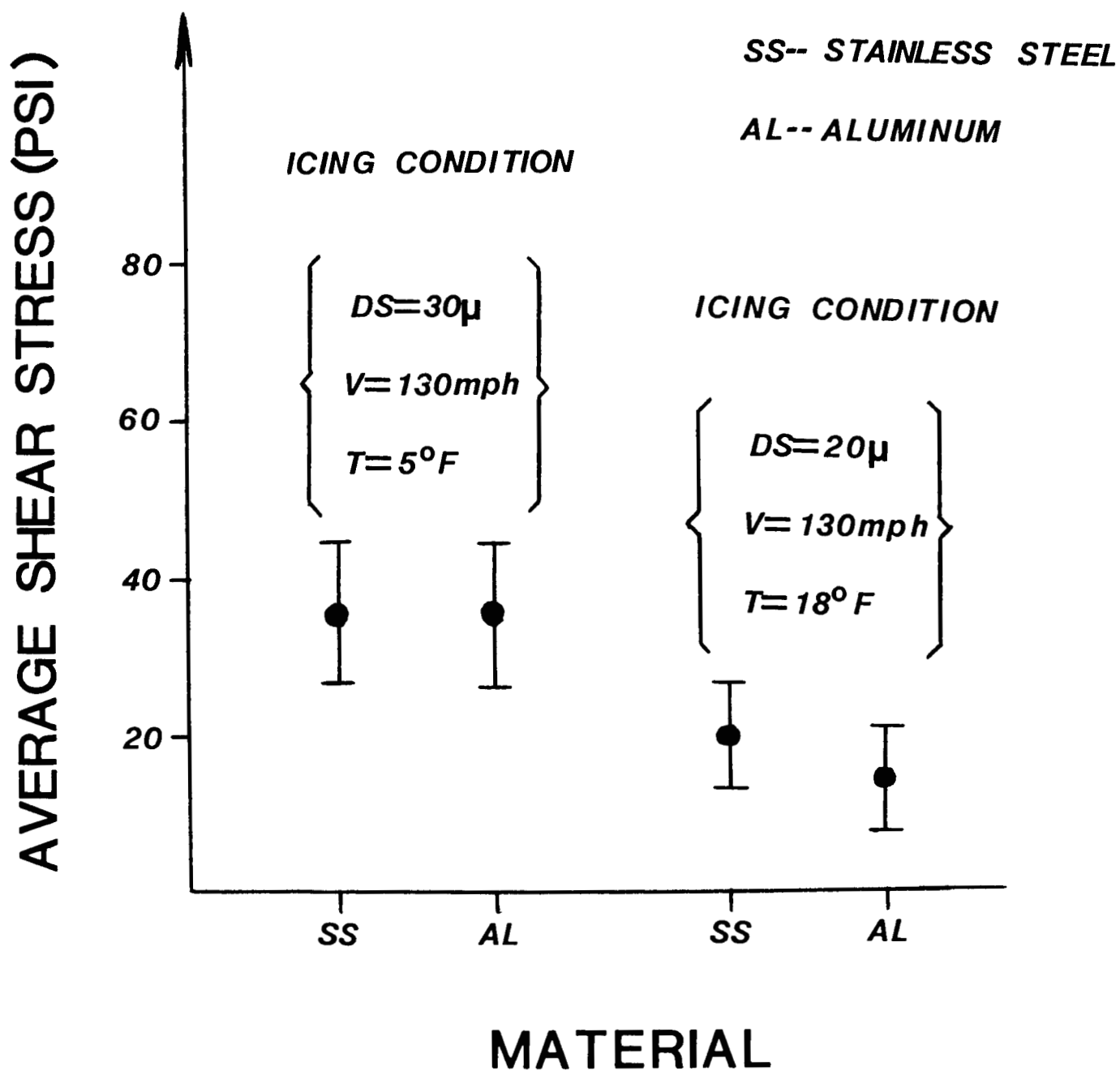
SS-- STAINLESS STEEL

AL-- ALUMINUM

ICING CONDITION

DS=30μ

V=130mph

T=5°F

ICING CONDITION

DS=20μ

V=130mph

T=18°F

AVERAGE SHEAR STRESS (PSI)

80

60

40

20

SS   AL   SS   AL

MATERIAL

FIG. 14 SHEAR STRESS VS.
MATERIAL SUBSTRATE

FIG. 15 SHEAR STRESS VS. WINDOW SHAPE

304 STAINLESS STEEL

SQUARE WINDOW

VELOCITY 130 mph

TEMPERATURE 18°F

DROP SIZE 30μ
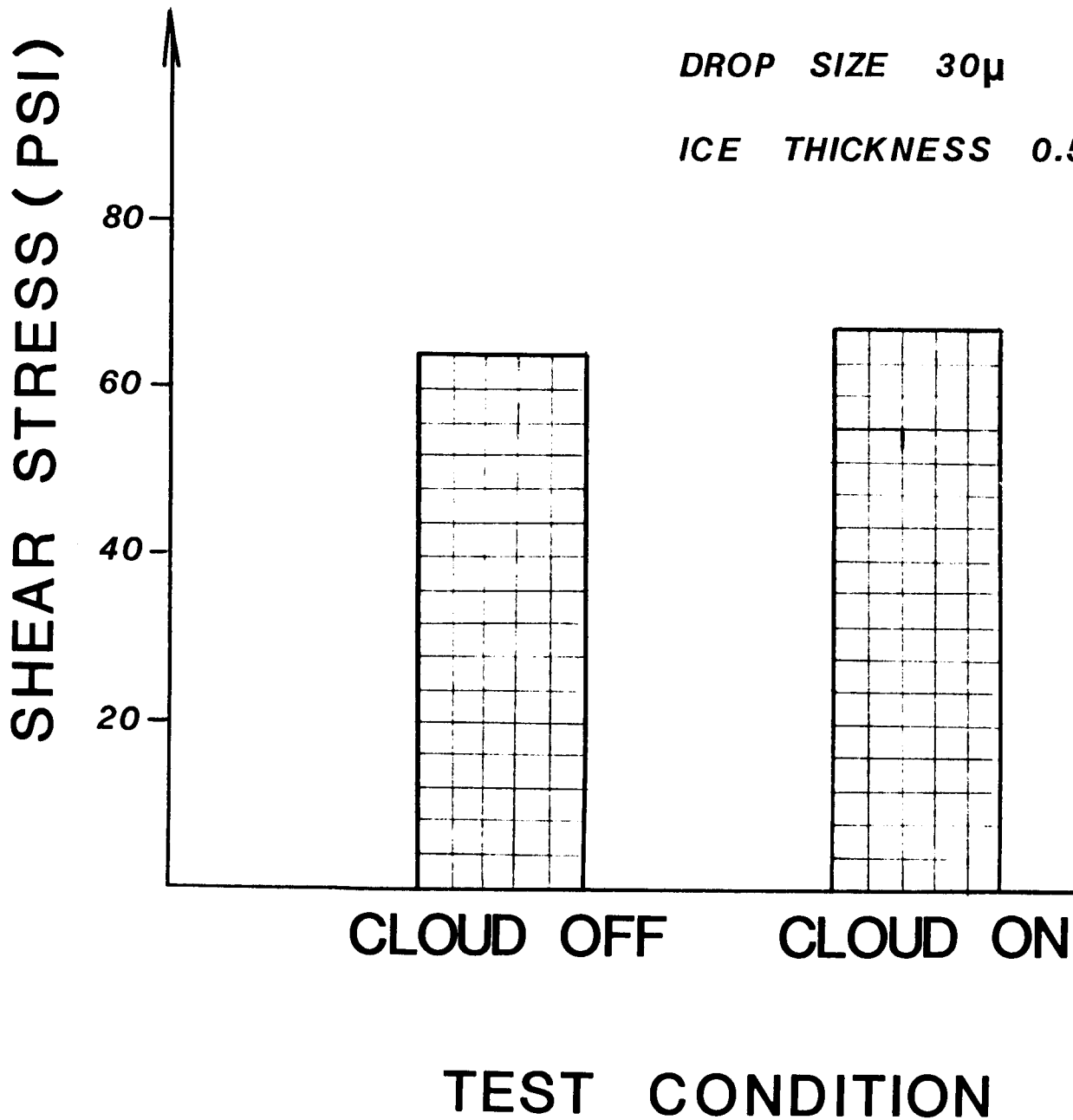
ICE THICKNESS 0.5"

FIG. 16 SHEAR STRESS
VS. TESTING CONDITION
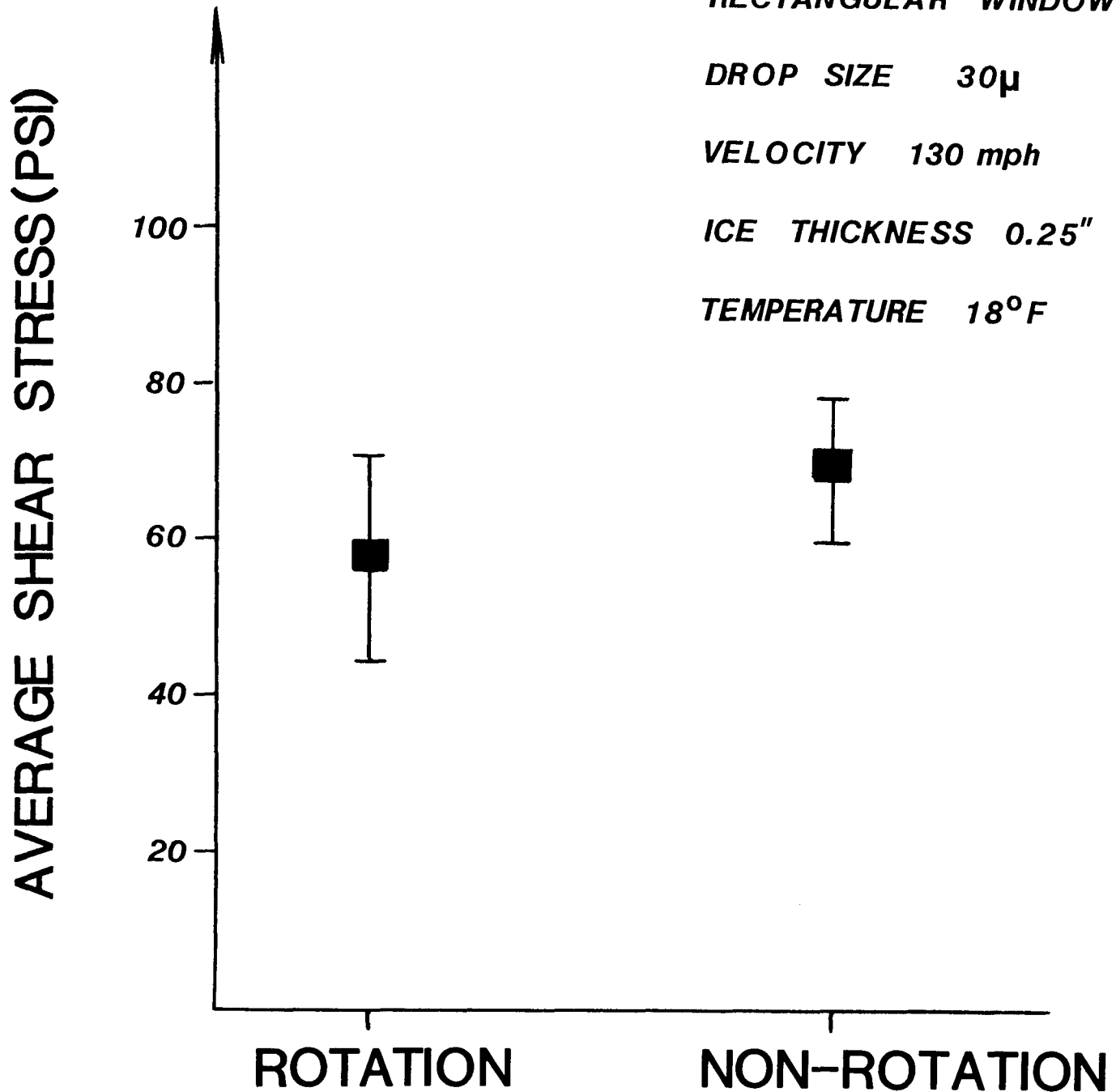
FIG. 17 SHEAR STRESS
VS. ICING CONDITION
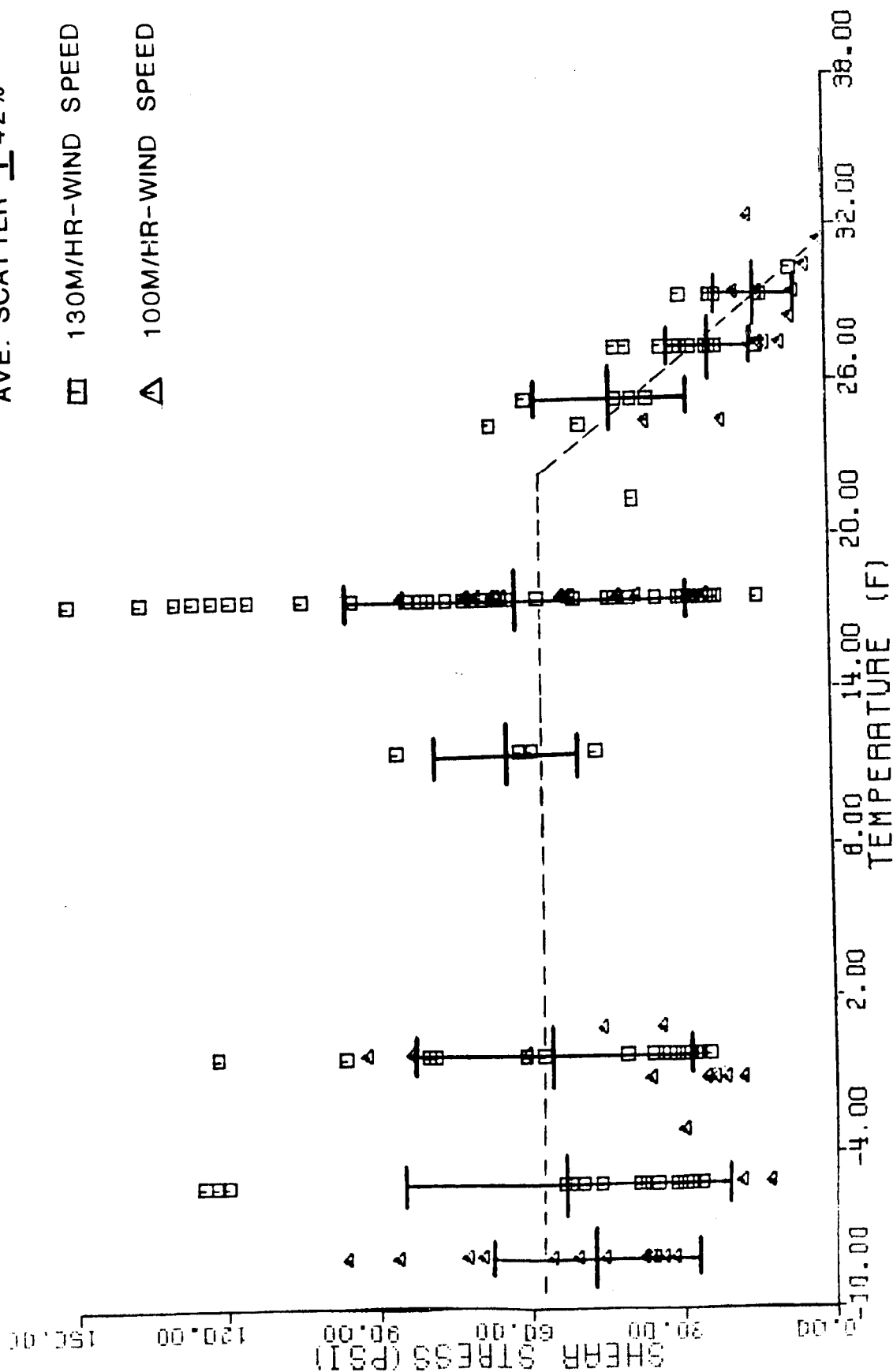
FIG.18 ADHESIVE SHEAR STRESS
VS. INTERFACE TEMPERATURE

40
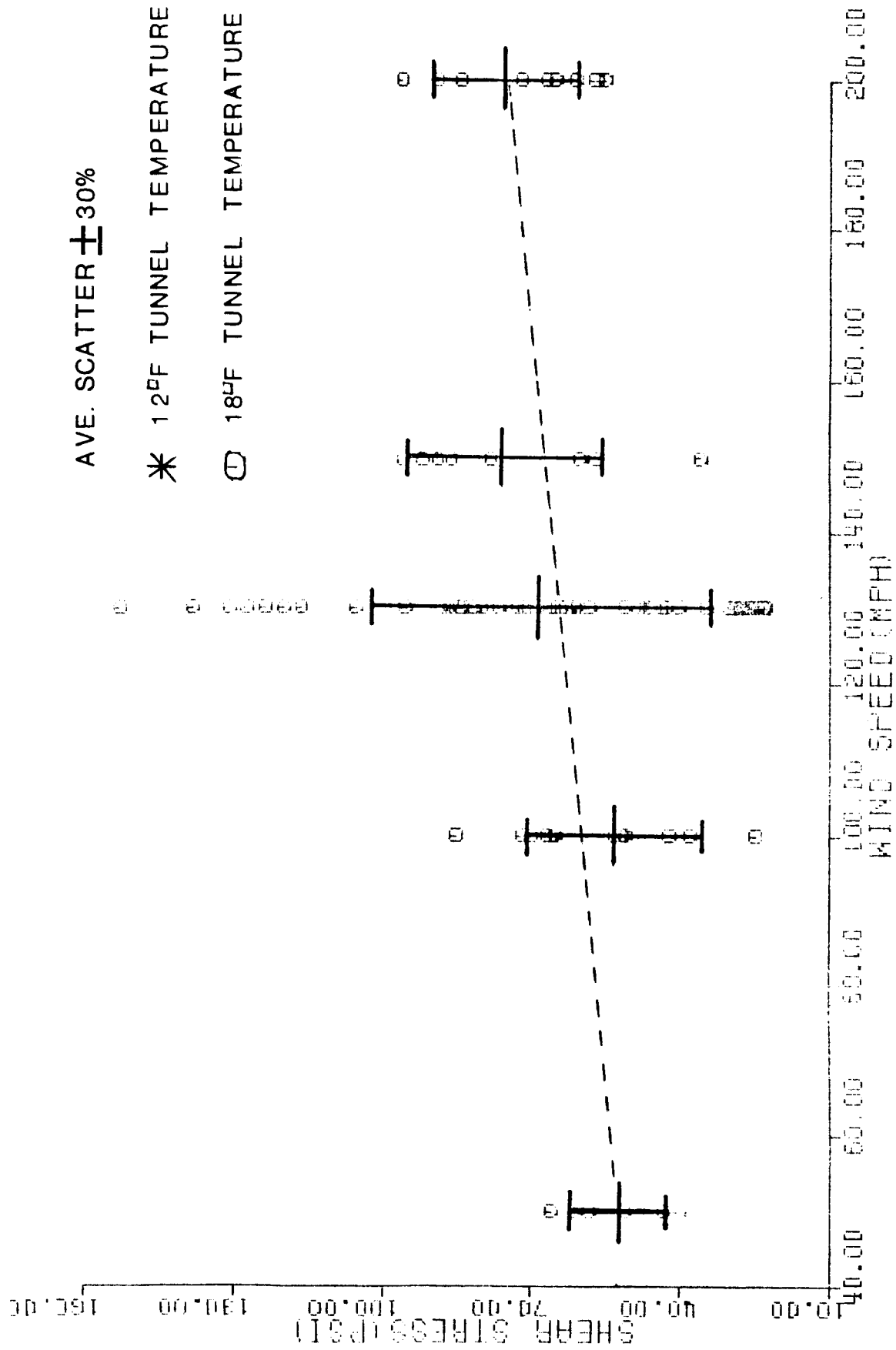
FIG.19   ADHESIVE SHEAR STRESS
VS. WIND VELOCITY

41

FIG. 20 ADHESIVE SHEAR STRESS
VS. WIND VELOCITY

SHEAR STRESS VS. DROPLET MOMENTUM

(12F TO 18F)

Shear Stress(PSI) : 175E-11⋅ Momentum +49.3

AVE. SCATTER ±13%

$V*D**3, FT**4/SEC \times 10**10$
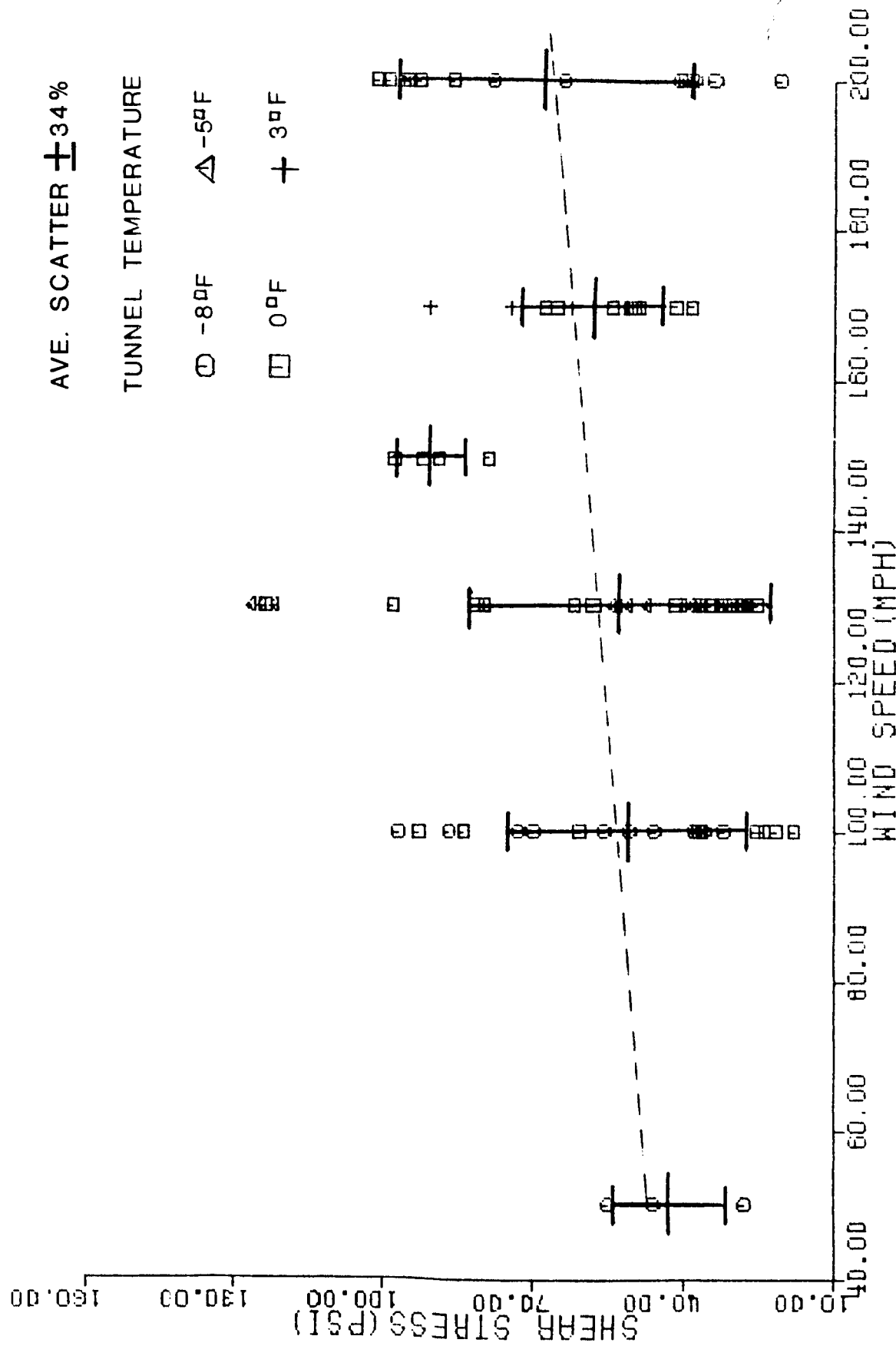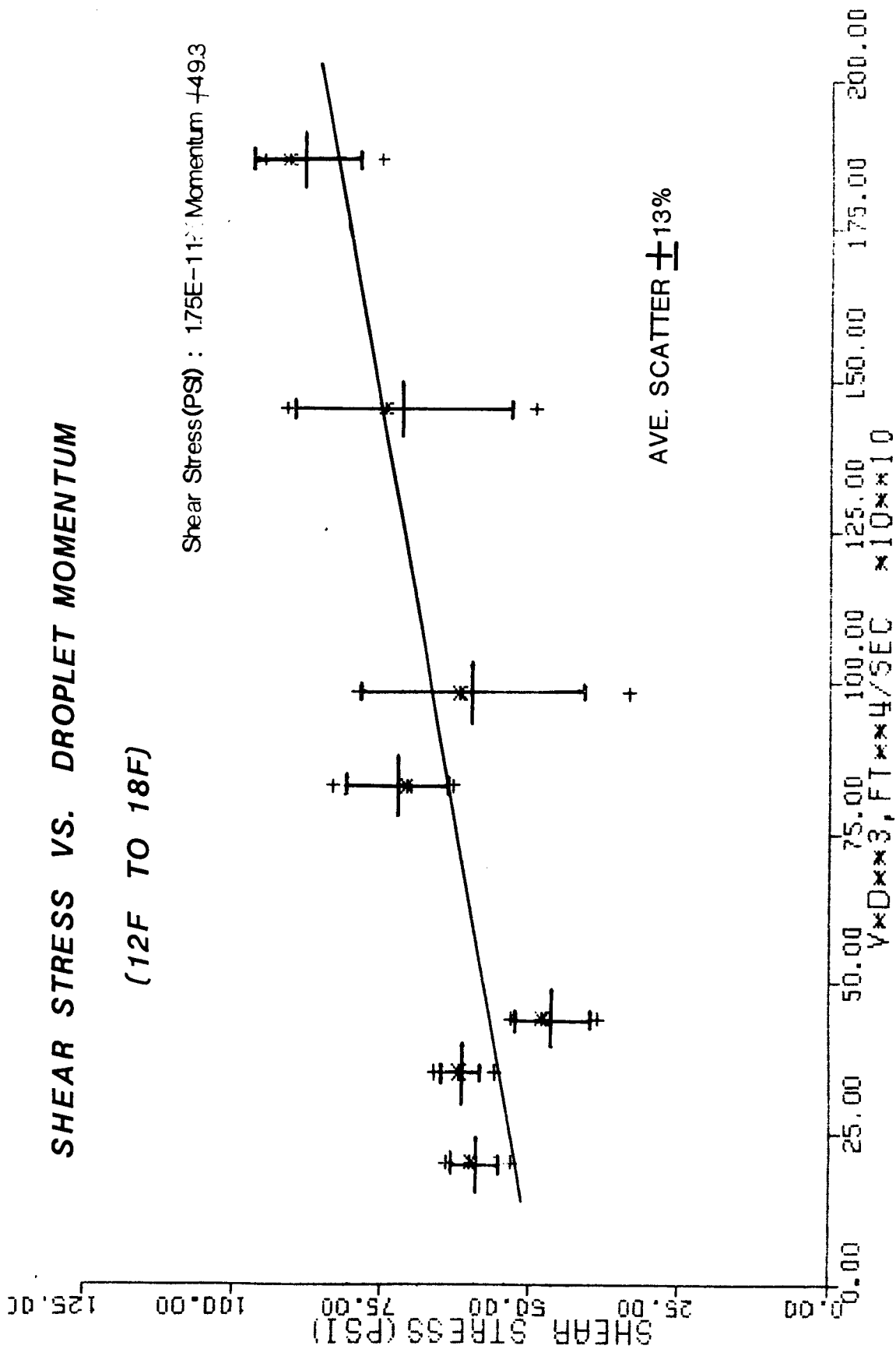
SHEAR STRESS (PSI)

FIGURE 21 STATISTICAL PLOT OF ADHESIVE SHEAR VS. DROPLET MOMENTUM
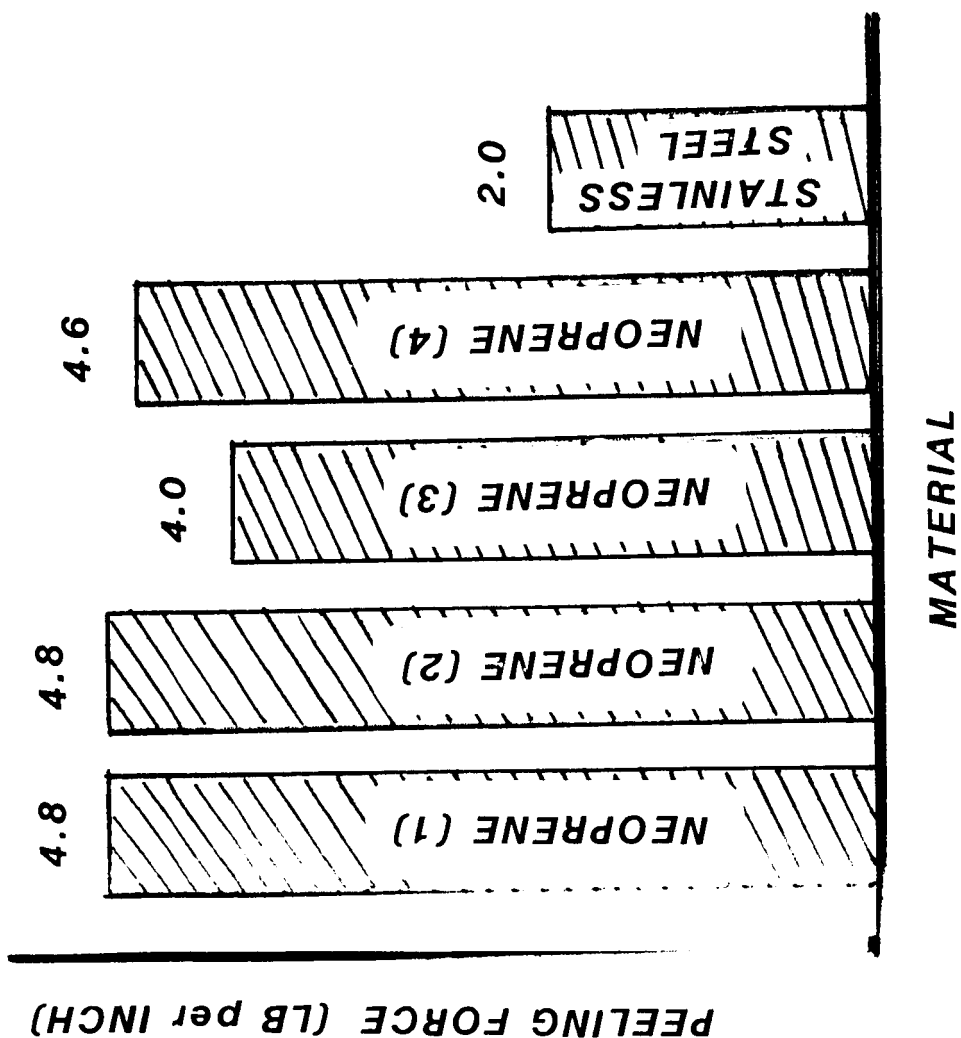
FIGURE 22 HISTOGRAM PLOT
OF PEELING TEST DATA

VERTICAL CENTER LINE

VERTICAL EDGE

HORIZONTAL CENTER LINE
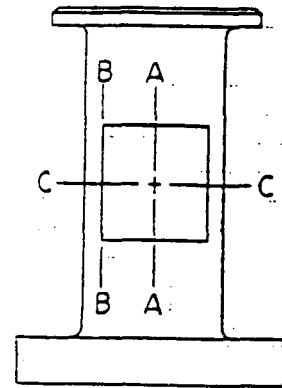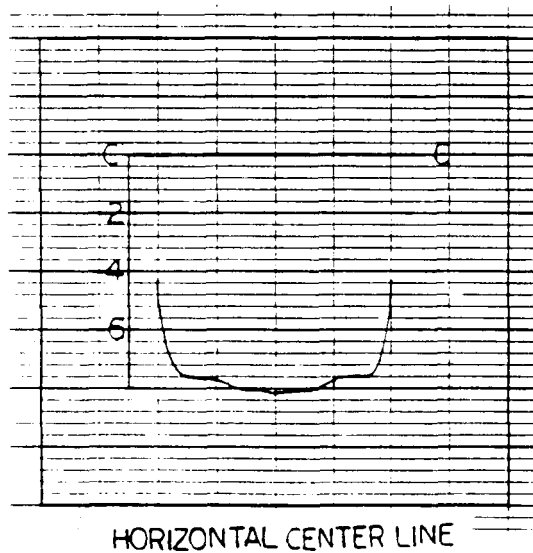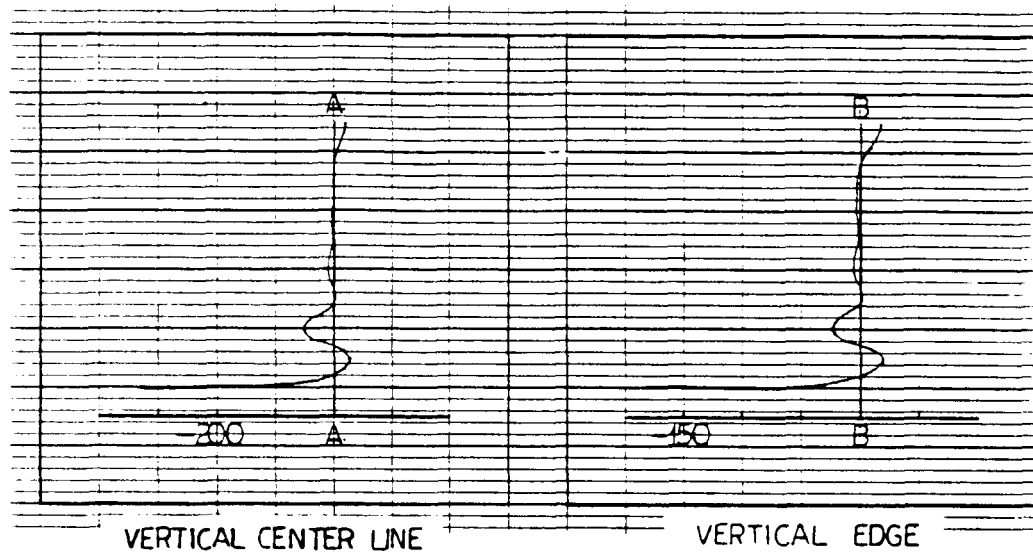
FIGURE 23 NORMAL STRESS DISTRIBUTION (SQUARE WINDOW)

VERTICAL CENTER LINE

VERTICAL EDGE

HORIZONTAL CENTER LINE
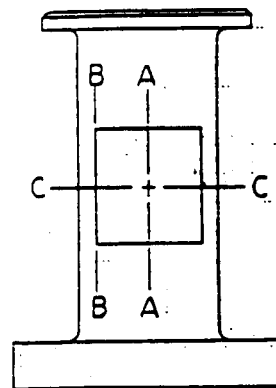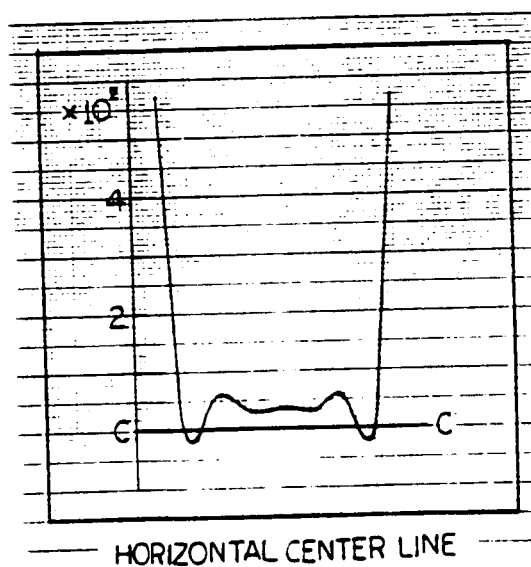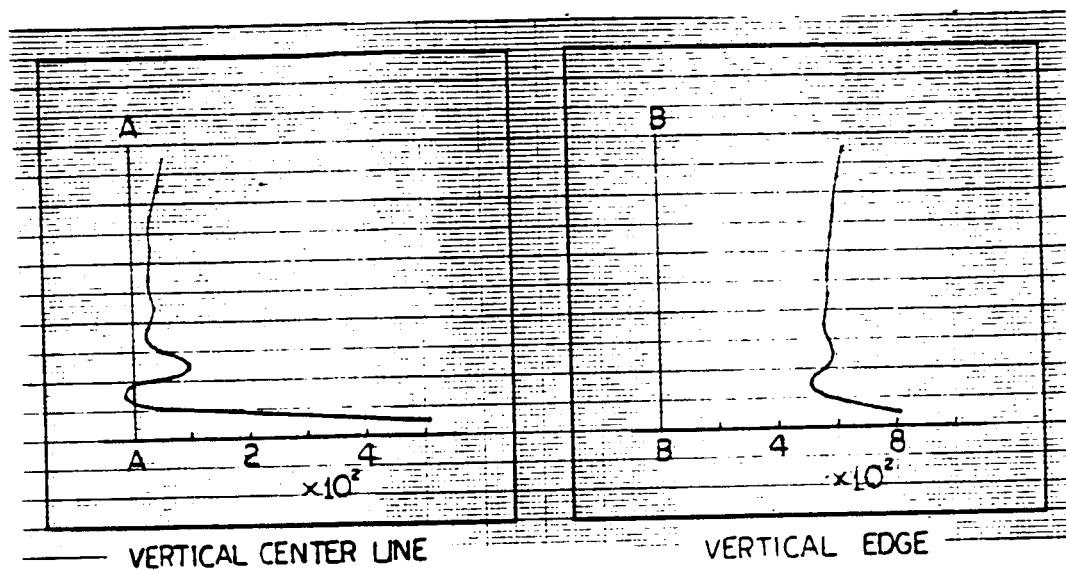
FIGURE 24 SHEAR STRESS DISTRIBUTION (SQUARE WINDOW)
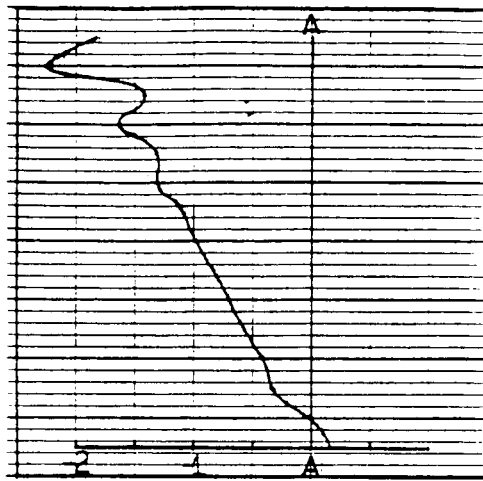
VERTICAL CENTER LINE
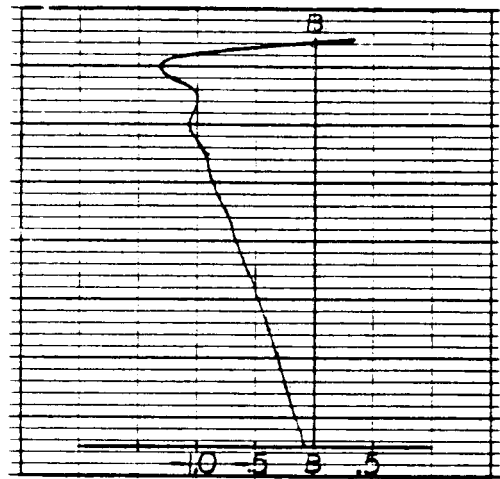
VERTICAL EDGE
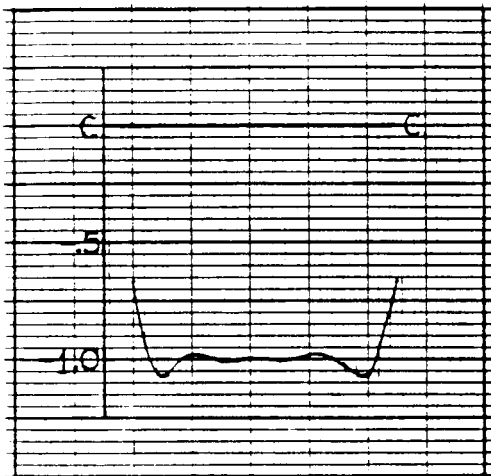
HORIZONTAL CENTER LINE
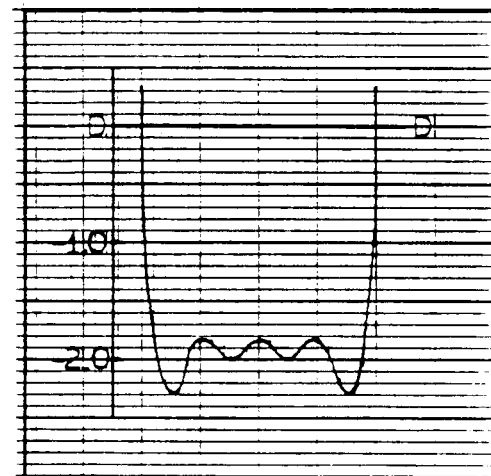
HORIZONTAL EDGE
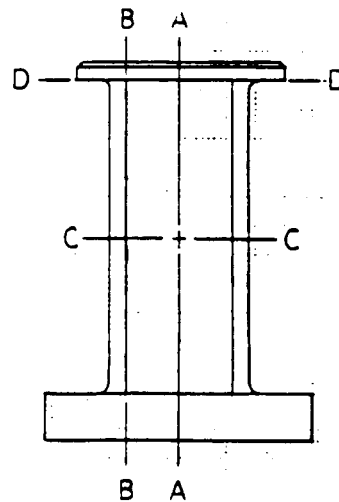
FIGURE 25 NORMAL STRESS DISTRIBUTION (RECTANGULAR WINDOW)

VERTICAL CENTER LINE

VERTICAL EDGE

HORIZONTAL CENTER LINE

HORIZONTAL EDGE
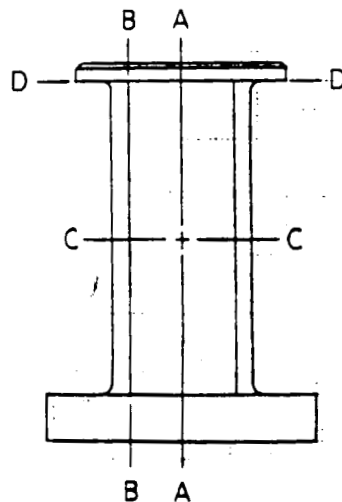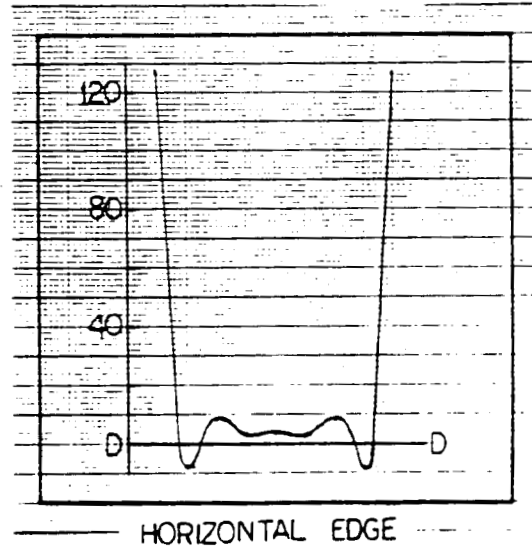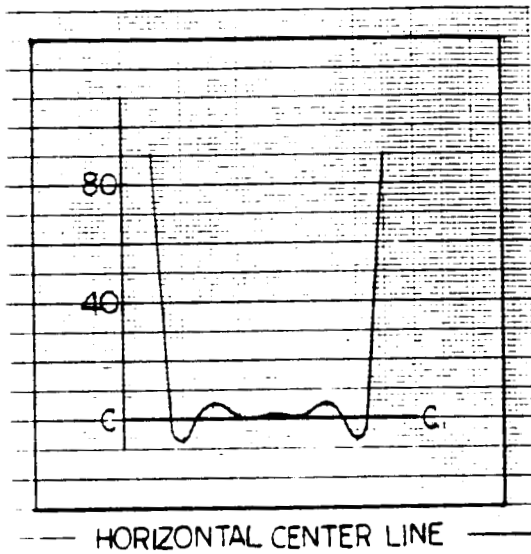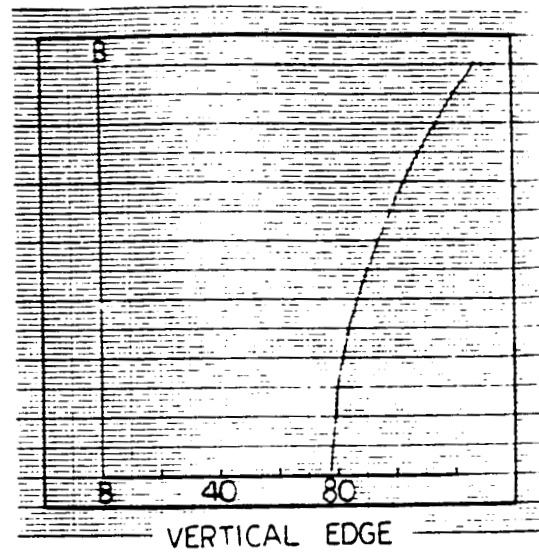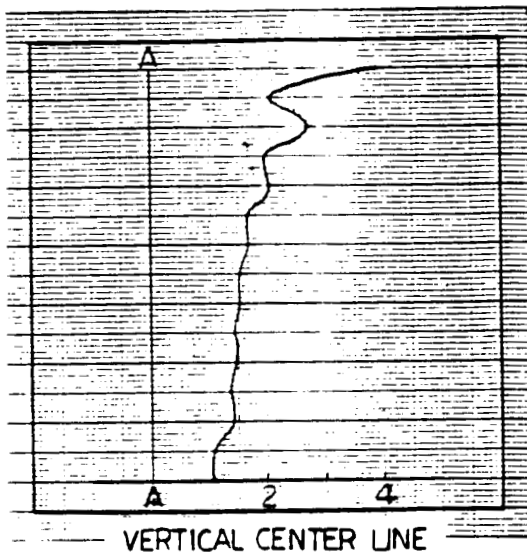
FIGURE 26 SHEAR STRESS DISTRIBUTION(RECTANGULAR WINDOW)
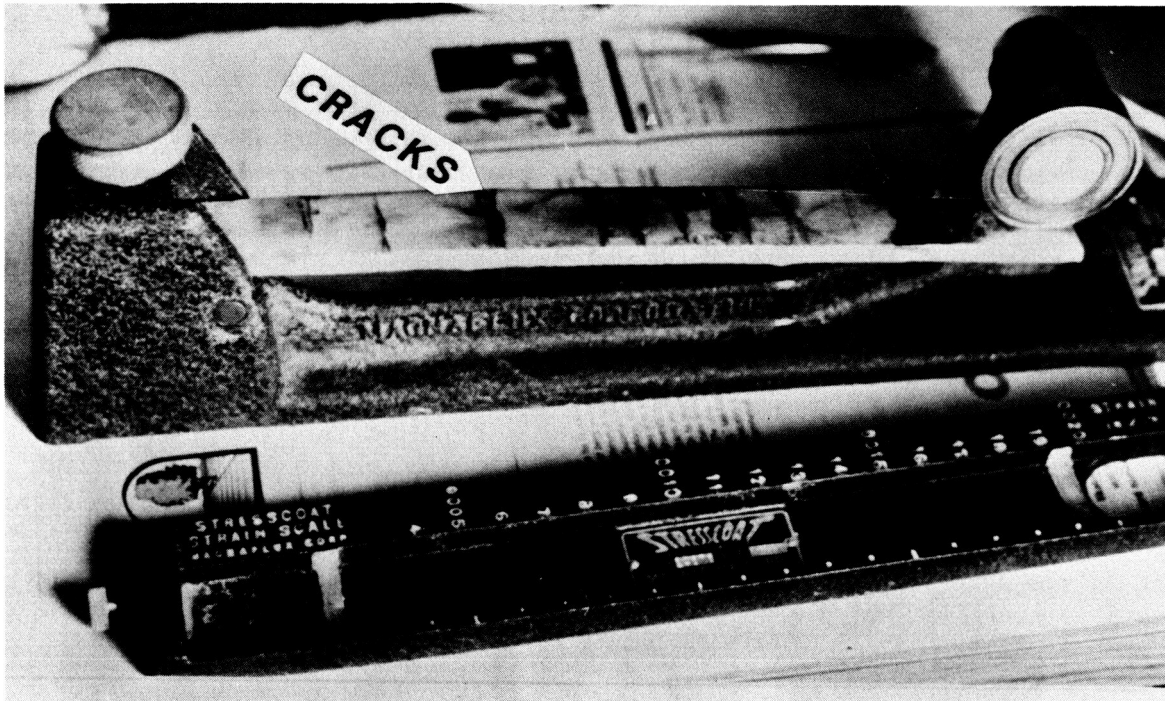
STRESS COAT STRAIN INDICATOR

ICE THICKNESS $= 0.1''$

DEFLECTION $= 0.625''$
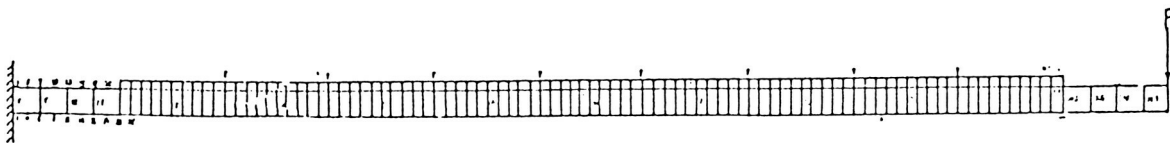
FINITE ELEMENT MODEL OF ICE COATED CANTILEVER BEAM

FIG. 27 BENDING FRACTURE TEST

APPENDIX

DATA LISTING

The following computer output is a comprehensive listing of data obtained in all experiments performed inside the NASA Icing Research Tunnel (IRT) facility. Statistical averages presented in this report are based on these data.

Codes used:

```
JO----- TUNNEL JOB NUMBER
RN----- RUN NUMBER
SN----- SPECIMEN NUMBER
CM----- CYLINDER MATERIAL (N:NEOPRENE;M:METAL;P:PLASTIC (ISFG))
WG----- WINDOW GEOMETRY
WC----- WATER CONTENT    (GRAMS PER CUBIC METER)
WS----- WIND SPEED    (MILES PER HOUR)
T ----- TOTAL TUNNEL TEMPERATURE    (DEGRESS FAHRENHEIT)
IT----- ICE THICKNESS    (INCHES)
ST----- SPRAY TIME  (MINUTES)
DS----- DROP SIZE(MICRONS)
OC----- OSCILLOSOPE CALIBRATION    (POUNDS FORCE PER DIVISION)
OR----- OSCILLOSOPE READING  (DIVISION)
TAU---- SHEAR STRESS    (POUNDS PER SQUARE INCH)
TT----- THEMOCOUPLE TEMPERATURE    (DEGRESS FAHRENHEIT)
AF----- ADDITIONAL INFORMATION
        CF-- CLOUD OFF TEST
        CN-- CLOUD ON TEST
        T -- CYLINDER MARKED ON TOP
        S -- CYLINDER MARKED ON SIDE
        R -- ROTATED SPECIMENS
        N -- NON-ROTATED SPECIMENS
        RR-- ROTATED SPECIMENS, STATE OF ICE:RIME
        RG-- ROTATED SPECIMENS, STATE OF ICE:GLAZE
        NR-- NON-ROTATED SPECIMENS,STATE OF ICE:RIME
        NG-- NON-ROTATED SPECIMENS,STATE OF ICE:GLAZE
        N*-- NON-ROTATED SPECIMENS,STATE OF ICE:SIDES-RIME,CENTER-
             -GLAZE
```

JO	RN	SN	CM	WG	WC	WS	T	IT	ST	DS	OC	OR	TAU	AF
6378	1	1	AL	RE	1.30	130.	18.	.2500	8.	20.	2.5	14.0	25.5	R
6378	1	2	AL	RE	1.30	130.	18.	.2500	8.	20.	2.5	19.0	34.6	R
6378	1	3	AL	RE	1.30	130.	18.	.2500	8.	20.	2.5	16.5	30.0	R
6378	1	4	AL	RE	1.30	130.	18.	.2500	8.	20.	2.5	14.0	25.5	R
6379	1	1	SS	RE	1.30	130.	18.	.3750	12.	20.	2.5	13.5	24.6	R
6379	1	2	SS	RE	1.30	130.	18.	.3750	12.	20.	2.5	14.5	26.4	R
6379	1	3	SS	RE	1.30	130.	18.	.3750	12.	20.	2.5	16.0	29.1	R
6379	1	4	SS	RE	1.30	130.	18.	.3750	12.	20.	2.5	22.0	40.0	R
6379	1	5	SS	RE	1.30	130.	18.	.3750	12.	20.	2.5	13.0	23.6	R
6379	2	1	AL	RE	1.30	130.	18.	.5000	16.	20.	2.5	15.5	28.2	R
6379	2	2	AL	RE	1.30	130.	18.	.5000	16.	20.	2.5	14.0	25.5	R
6379	2	3	AL	RE	1.30	130.	18.	.5000	16.	20.	2.5	23.5	42.7	R
6379	4	1	AL	RE	1.30	130.	18.	.3750	12.	20.	5.0	7.0	25.5	R
6379	4	2	AL	RE	1.30	130.	18.	.3750	12.	20.	5.0	4.0	14.6	R
6379	4	3	AL	RE	1.30	130.	18.	.3750	12.	20.	5.0	7.5	27.3	R
6379	4	4	AL	RE	1.30	130.	18.	.3750	12.	20.	5.0	6.3	22.9	R
6379	4	5	AL	RE	1.30	130.	18.	.3750	12.	20.	5.0	7.0	25.5	R
6379	5	2	SS	RE	1.30	130.	-5.	.3750	12.	20.	5.0	7.5	27.3	R
6379	5	3	SS	RE	1.30	130.	-5.	.3750	12.	20.	5.0	11.0	40.0	R
6379	5	4	SS	RE	1.30	130.	-5.	.3750	12.	20.	5.0	8.5	30.9	R
6379	7	1	SS	RE	2.22	130.	-5.	.7500	10.	30.	10.0	6.5	47.3	R
6379	7	2	SS	RE	2.22	130.	-5.	.7500	10.	30.	10.0	7.3	53.1	R
6379	7	3	SS	RE	2.22	130.	-5.	.7500	10.	30.	10.0	5.0	36.4	R
6379	8	1	AL	RE	2.22	130.	-5.	.7500	10.	30.	10.0	5.0	36.4	R
6379	8	2	AL	RE	2.22	130.	-5.	.7500	10.	30.	10.0	7.0	50.9	R
6379	8	4	AL	RE	2.22	130.	-5.	.7500	10.	30.	10.0	5.3	38.6	R
6379	8	5	AL	RE	2.22	130.	-5.	.7500	10.	30.	10.0	7.5	54.6	R
6380	4	1	SS	RE	2.22	130.	18.	.3750	6.	30.	10.0	17.0	123.7	R
6380	4	2	SS	RE	2.22	130.	18.	.3750	6.	30.	10.0	16.5	120.0	R
6380	4	3	SS	RE	2.22	130.	18.	.3750	6.	30.	10.0	19.0	138.2	R
6380	4	4	SS	RE	2.22	130.	18.	.3750	6.	30.	10.0	18.0	131.0	R
6380	6	1	SS	RE	2.22	130.	18.	.3750	6.	30.	10.0	14.5	105.5	R
6380	6	2	SS	RE	2.22	130.	18.	.3750	6.	30.	10.0	11.5	83.7	R
6380	6	3	SS	RE	2.22	130.	18.	.3750	6.	30.	10.0	21.0	152.8	R
6380	6	4	SS	RE	2.22	130.	18.	.3750	6.	30.	10.0	16.5	120.0	R
6380	6	5	SS	RE	2.22	130.	18.	.3750	6.	30.	10.0	16.0	116.4	R
6380	7	6	SS	RE	2.22	130.	0.	.5000	6.	30.	10.0	11.0	80.0	R
6380	7	8	SS	RE	2.22	130.	0.	.5000	6.	30.	10.0	8.0	58.2	R
6380	7	9	SS	RE	2.22	130.	0.	.5000	6.	30.	10.0	8.5	61.8	R
6380	7	10	SS	RE	2.22	130.	0.	.5000	6.	30.	10.0	11.0	80.0	R
6380	8	1	AL	RE	2.22	130.	0.	.5000	6.	30.	10.0	11.0	80.0	R
6380	8	2	AL	RE	2.22	130.	0.	.5000	6.	30.	10.0	11.2	81.5	R
6380	8	3	AL	RE	2.22	130.	0.	.5000	6.	30.	10.0	17.0	123.7	R
6380	8	4	AL	RE	2.22	130.	0.	.5000	6.	30.	10.0	13.5	98.2	R

JO	RN	SN	CM	WG	WC	WS	T	IT	ST	DS	OC	OR	TAU	AF
6381	4	1	SS	RE	2.22	130.	18.	.2500	2.	30.	10.0	11.2	81.5	N
6381	4	2	SS	RE	2.22	130.	18.	.2500	2.	30.	10.0	8.0	58.2	N
6381	4	3	SS	RE	2.22	130.	18.	.2500	2.	30.	10.0	9.0	65.5	N
6381	4	4	SS	RE	2.22	130.	18.	.2500	2.	30.	10.0	10.5	76.4	N
6381	4	5	SS	RE	2.22	130.	18.	.2500	2.	30.	10.0	9.5	69.1	N
6381	5	1	SS	RE	2.22	130.	18.	.2500	2.	30.	10.0	10.0	72.8	N
6381	5	2	SS	RE	2.22	130.	18.	.2500	2.	30.	10.0	11.0	80.0	N
6381	5	3	SS	RE	2.22	130.	18.	.2500	2.	30.	10.0	11.6	84.4	N
6381	5	4	SS	RE	2.22	130.	18.	.2500	2.	30.	10.0	10.0	72.8	N
6381	6	1	SS	RE	2.22	130.	18.	.2500	4.	30.	10.0	10.0	72.8	T
6381	6	2	SS	RE	2.22	130.	18.	.2500	4.	30.	10.0	7.0	50.9	T
6381	6	3	SS	RE	2.22	130.	18.	.2500	4.	30.	10.0	9.8	71.3	T
6381	6	4	SS	RE	2.22	130.	18.	.2500	4.	30.	10.0	6.0	43.7	T
6381	6	5	SS	RE	2.22	130.	18.	.2500	4.	30.	10.0	7.0	50.9	T
6381	7	6	SS	SG	2.22	130.	18.	.2500	4.	30.	10.0	6.7	64.0	S
6381	7	7	SS	SG	2.22	130.	18.	.2500	4.	30.	10.0	10.0	95.5	S
6381	7	8	SS	SG	2.22	130.	18.	.2500	4.	30.	10.0	7.2	68.8	S
6381	8	1	AL	RE	2.22	130.	18.	.2500	4.	30.	10.0	18.0	131.0	T
6381	8	2	AL	RE	2.22	130.	18.	.2500	4.	30.	10.0	17.5	127.3	T
6382	1	1	SS	SG	2.22	130.	18.	.5000	8.	30.	10.0	6.7	64.0	CF
6382	2	1	SS	RE	2.22	130.	18.	.5000	5.	30.	10.0	8.0	58.2	CN
6382	3	6	SS	RE	2.22	130.	18.	.5000	5.	30.	10.0	8.8	64.0	CF
6382	4	1	SS	SG	2.22	130.	18.	.5000	5.	30.	10.0	7.0	66.8	CN
6382	5	7	SS	RE	1.30	130.	-5.	.3125	8.	20.	10.0	5.0	36.4	S
6382	5	8	SS	RE	1.30	130.	-5.	.3125	8.	20.	10.0	4.5	32.7	S
6382	5	10	SS	RE	1.30	130.	-5.	.3125	8.	20.	10.0	5.0	36.4	S
6382	6	1	SS	RE	1.30	130.	-5.	.3125	8.	20.	5.0	7.5	27.3	T
6382	6	2	SS	RE	1.30	130.	-5.	.3125	8.	20.	5.0	8.0	29.1	T
6382	7	2	SS	SG	1.30	130.	-5.	.3125	8.	20.	5.0	26.0	124.1	S
6382	7	3	SS	SG	1.30	130.	-5.	.3125	8.	20.	5.0	26.5	126.5	S
6382	7	4	SS	SG	1.30	130.	-5.	.3125	8.	20.	5.0	25.5	121.8	S
6383	4	1	SS	RE	1.30	130.	0.	.2500	8.	20.	5.0	8.3	30.2	T
6383	4	2	SS	RE	1.30	130.	0.	.2500	8.	20.	5.0	9.5	34.6	T
6383	4	3	SS	RE	1.30	130.	0.	.2500	8.	20.	5.0	9.0	32.7	T
6383	4	4	SS	RE	1.30	130.	0.	.2500	8.	20.	5.0	9.0	32.7	T
6383	4	5	SS	RE	1.30	130.	0.	.2500	8.	20.	5.0	7.0	25.5	T
6383	5	6	SS	RE	1.30	130.	0.	.2500	8.	20.	5.0	8.5	30.9	S
6383	5	7	SS	RE	1.30	130.	0.	.2500	8.	20.	5.0	7.5	27.3	S
6383	5	8	SS	RE	1.30	130.	0.	.2500	8.	20.	5.0	8.0	29.1	S
6383	5	10	SS	RE	1.30	130.	0.	.2500	8.	20.	5.0	10.0	36.4	S
6383	6	1	SS	RE	1.30	130.	0.	.2500	8.	20.	5.0	7.8	28.4	T
6383	6	2	SS	RE	1.30	130.	0.	.2500	8.	20.	5.0	8.0	29.1	T
6383	6	4	SS	RE	1.30	130.	0.	.2500	8.	20.	5.0	11.5	41.8	T
6383	6	5	SS	RE	1.30	130.	0.	.2500	8.	20.	5.0	10.0	36.4	T
6383	7	6	SS	RE	1.30	170.	0.	.3125	8.	20.	5.0	18.0	65.5	S

JO	RN	SN	CM	WG	WC	WS	T	IT	ST	DS	OC	OR	TAU	AF
6383	7	7	SS	RE	1.30	170.	0.	.3125	8.	20.	5.0	13.5	49.1	S
6383	7	8	SS	RE	1.30	170.	0.	.3125	8.	20.	5.0	13.8	50.2	S
6383	7	9	SS	RE	1.30	170.	0.	.3125	8.	20.	5.0	11.5	41.8	S
6383	7	10	SS	RE	1.30	170.	0.	.3125	8.	20.	5.0	13.5	49.1	S
6383	10	1	SS	RE	1.30	170.	3.	.5000	8.	20.	5.0	20.5	74.6	T
6383	10	2	SS	RE	1.30	170.	3.	.5000	8.	20.	5.0	17.2	62.6	T
6383	10	3	SS	RE	1.30	170.	3.	.5000	8.	20.	5.0	16.0	58.2	T
6383	10	4	SS	RE	1.30	170.	3.	.5000	8.	20.	5.0	14.2	51.7	T
6383	10	5	SS	RE	1.30	170.	3.	.5000	8.	20.	5.0	25.0	90.9	T
6383	11	7	SS	RE	1.30	170.	0.	.5000	8.	20.	10.0	5.3	38.6	S
6383	11	8	SS	RE	1.30	170.	0.	.5000	8.	20.	10.0	9.3	67.7	S
6383	11	9	SS	RE	1.30	170.	0.	.5000	8.	20.	10.0	7.0	50.9	S
6383	11	10	SS	RE	1.30	170.	0.	.5000	8.	20.	10.0	7.5	54.6	S
6383	12	1	SS	RE	1.30	100.	-1.	.3125	8.	20.	10.0	2.5	18.2	T
6383	12	2	SS	RE	1.30	100.	-1.	.3125	8.	20.	10.0	3.5	25.5	T
6383	12	3	SS	RE	1.30	100.	-1.	.3125	8.	20.	10.0	3.0	21.8	T
6383	12	4	SS	RE	1.30	100.	-1.	.3125	8.	20.	10.0	5.0	36.4	T
6383	12	5	SS	RE	1.30	100.	-1.	.3125	8.	20.	10.0	3.3	24.0	T

JO	RN	SN	CM	WG	WC	WS	T	IT	ST	DS	OR	OR	TAU	AF
6384	1	1	SS	RE	1.7	100.	18.	.3750	13.6	26.6	3.55	70.	51.	
6384	1	2	SS	RE	1.7	100.	18.	.3750	13.6	26.6	5.0	116.	85.	
6384	1	3	SS	RE	1.7	100.	18.	.3750	13.6	26.6	1.4	35.	25.	
6384	1	4	SS	RE	1.7	100.	18.	.3750	13.6	26.6	1.4	35.	25.	
6384	1	5	SS	RE	1.7	100.	18.	.3750	13.6	26.6	1.4	35.	25.	
6384	2	1	SS	RE	1.7	100.	18.	.2500	8.	26.6	4.0	88.	65.	
6384	2	2	SS	RE	1.7	100.	18.	.2500	8.	26.6	5.0	99.	72.	
6384	2	3	SS	RE	1.7	100.	18.	.2500	8.	26.6	4.6	91.	66.	
6384	2	4	SS	RE	1.7	100.	18.	.2500	8.	26.6	4.9	97.	70.	
6384	3	1	SS	RE	1.7	150.	18.	.2500	8.	26.6	5.4	107.	78.	
6384	3	2	SS	RE	1.7	150.	18.	.2500	8.	26.6	2.5	49.	36.	
6384	3	3	SS	RE	1.7	150.	18.	.2500	8.	26.6	6.4	126.	92.	
6384	3	4	SS	RE	1.7	150.	18.	.2500	8.	26.6	4.0	79.	57.	
6384	3	5	SS	RE	1.7	150.	18.	.2500	8.	26.6	6.2	122.	89.	
6384	4	1	SS	RE	1.7	150.	18.	.2500	8.	26.6	6.7	132.	96.	
6384	4	2	SS	RE	1.7	150.	18.	.2500	8.	26.6	6.0	118.	86.	
6384	4	4	SS	RE	1.7	150.	18.	.2500	8.	26.6	4.6	91.	60.	
6384	6	3	SS	RE	1.7	200.	18.	.3750	4.	26.6	6.7	132.	96.	
6384	6	4	SS	RE	1.7	200.	18.	.3750	4.	26.6	6.2	122.	89.	
6384	6	5	SS	RE	1.7	200.	18.	.3750	4.	26.6	6.7	132.	96.	
6384	7	1	SS	RE	1.7	100.	0.	.3750	4.	26.6	4.6	91.	61.	
6384	7	2	SS	RE	1.7	150.	0.	.3750	4.	26.6	5.5	109.	79.	
6384	7	3	SS	RE	1.7	100.	0.	.3750	4.	26.6	6.5	128.	93.	
6384	7	4	SS	RE	1.7	100.	0.	.3750	4.	26.6	5.85	115.	84.	
6384	8	1	SS	RE	1.7	150.	0.	.3750	4.	26.6	6.4	126.	92.	
6384	8	2	SS	RE	1.7	150.	0.	.3750	4.	26.6	6.2	122.	89.	

JO	RN	SN	CM	WG	WC	WS	T	IT	ST	DS	OC	OR	TAU	AF
6384	8	4	SS	RE	1.7	150.	0.	.3750	4.	26.6	6.8	134.	98.	
6384	8	5	SS	RE	1.7	150.	0.	.3750	4.	26.6	6.8	134.	98.	
6384	9	1	SS	RE	1.7	200.	0.	.3750	4.	26.6	6.9	136.	99.	
6384	9	2	SS	RE	1.7	200.	0.	.3750	4.	26.6	6.9	136.	99.	
6384	9	3	SS	RE	1.7	200.	0.	.3750	4.	26.6	6.6	130.	95.	
6384	9	4	SS	RE	1.7	200.	0.	.3750	4.	26.6	6.7	132.	96.	
6384	9	5	SS	RE	1.7	200.	0.	.3750	4.	26.6	6.7	132.	96.	
6384	10	1	SS	RE	1.7	200.	0.	.3750	4.	26.6	7.0	138.	101.	
6384	10	3	SS	RE	1.7	200.	0.	.3750	4.	26.6	6.0	118.	86.	
6384	10	4	SS	RE	1.7	200.	0.	.3750	4.	26.6	6.5	128.	93.	
6384	10	5	SS	RE	1.7	200.	0.	.3750	4.	26.6	6.6	130.	95.	

JO	RN	SN	CM	WG	WC	WS	T	IT	ST	DS	OR	OR	TAU	TT
6385	2	2	AL	RE	1.31	130.	0.	.2500	8.	20.0	3.4	67.	49.	25.
6385	2	3	AL	RE	1.31	130.	0.	.2500	8.	20.0	0.5	10.	7.1	31.
6385	2	4	AL	RE	1.31	130.	0.	.2500	8.	20.0	4.7	93.	67.	25.
6385	2	5	AL	RE	1.31	130.	0.	.2500	8.	20.0	2.9	57.	42.	26.
6385	3	2	304	RE	1.31	130.	0.	.2500	8.	20.0	2.7	53.	39.	22.
6385	4	2	304	RE	1.31	130.	0.	.2500	8.	20.0	1.0	20.	14.	28.
6385	4	3	304	RE	1.31	130.	0.	.2500	8.	20.0	0.0	0.	0.	40.
6385	4	4	304	RE	1.31	130.	0.	.2500	8.	20.0	23.	45.	33.	28.
6386	1	1	SS	RE	1.31	130.	12.	.3125	10.	19.7	1.9	38.	27.	28.
6386	1	2	SS	RE	1.31	130.	12.	.3125	10.	19.7	1.6	32.	23.	28.
6386	1	4	SS	RE	1.31	130.	12.	.3125	10.	19.7	1.7	33.	24.	28.
6386	2	1	AL	RE	1.31	130.	12.	.3125	10.	19.7	0.9	18.	13.	30.
6386	2	2	AL	RE	1.31	130.	12.	.3125	10.	19.7	1.5	30.	22.	30.
6386	2	3	AL	RE	1.31	130.	12.	.3125	10.	19.7	2.0	39.	29.	30.
6386	2	4	AL	RE	1.31	130.	12.	.3125	10.	19.7	1.6	32.	23.	30.
6386	2	5	AL	RE	1.31	130.	12.	.3125	10.	19.7	1.6	32.	23.	30.
6386	3	3	SS	RE	1.31	130.	12.	.3125	10.	19.7	4.2	83.	60.	26.
6386	3	4	SS	RE	1.31	130.	12.	.3125	10.	19.7	2.5	49.	36.	26.
6386	3	5	SS	RE	1.31	130.	12.	.3125	10.	19.7	2.7	53.	39.	26.
6386	4	1	AL	RE	1.31	130.	12.	.3125	10.	19.7	1.0	20.	14.	28.
6386	4	2	AL	RE	1.31	130.	12.	.3125	10.	19.7	2.8	55.	40.	28.
6386	4	4	AL	RE	1.31	130.	12.	.3125	10.	19.7	2.9	57.	42.	28.
6386	5	1	AL	RE	1.31	130.	12.	.3125	10.	19.7	1.5	30.	22.	28.
6386	5	2	AL	RE	1.31	130.	12.	.3125	10.	19.7	2.0	39.	29.	28.
6386	5	3	AL	RE	1.31	130.	12.	.3125	10.	19.7	1.7	34.	24.	28.
6386	5	4	AL	RE	1.31	130.	12.	.3125	10.	19.7	2.1	41.	30.	28.
6386	7	1	N	S	1.31	130.	12.	.3125	12.	19.7	2.5	49.	47.	12.
6386	7	2	N	S	1.31	130.	12.	.3125	12.	19.7	3.2	63.	60.	12.
6386	7	3	P	S	1.31	130.	12.	.3125	12.	19.7	4.6	91.	87.	12.
6386	7	5	M	S	1.31	130.	12.	.3125	12.	19.7	3.3	65.	62.	12.
6386	10	1	AL	RE	1.00	170.	13.	.3125	12.	19.7	2.0	39.	29.	12.
6386	10	2	AL	RE	1.00	170.	13.	.3125	12.	19.7	2.0	39.	29.	12.
6386	10	3	AL	RE	1.00	170.	13.	.3125	12.	19.7	1.85	37.	27.	12.

JO	RN	SN	CM	WG	WC	WS	T	IT	ST	DS	OC	OR	TAU	AF
6386	10	4	AL	RE	1.00	170.	13.	.3125	12.	19.7	4.1	81.	59.	12.
6386	10	5	AL	RE	1.00	170.	13.	.3125	12.	19.7	1.8	36.	26.	12.

JO	RN	SN	CM	WG	WC	WS	T	IT	ST	DS	OR	FOR	AUF	AF
6387	1	1	SS	RE	3.55	50.	18.	.1250	8.	20.0		70.	51.	RG
6387	1	2	SS	RE	3.55	50.	18.	.1250	8.	20.0		84.	61.	RG
6387	1	3	SS	RE	3.55	50.	18.	.1250	8.	20.0		80.	58.	RG
6387	1	4	SS	RE	3.55	50.	18.	.1250	8.	20.0		90.	66.	RG
6387	2	1	AL	RE	2.30	50.	18.	.3750	12.	15.0		44.	61.	NR
6387	2	2	AL	RE	2.30	50.	18.	.3750	12.	15.0		55.	40.	NR
6387	2	3	AL	RE	2.30	50.	18.	.3750	12.	15.0		55.	40.	NR
6387	2	4	AL	RE	2.30	50.	18.	.3750	12.	15.0		60.	43.	NR
6387	2	5	AL	RE	2.30	50.	18.	.3750	12.	15.0		70.	51.	NR
6387	3	1	AL	RE	1.77	100.	18.	.6250	8.	20.0		73.	53.	N
6387	3	2	AL	RE	1.77	100.	18.	.6250	8.	20.0		53.	38.	N
6387	3	3	AL	RE	1.77	100.	18.	.6250	8.	20.0		71.	53.	N
6387	3	4	AL	RE	1.77	100.	18.	.6250	8.	20.0		71.	52.	N
6387	3	5	AL	RE	1.77	100.	18.	.6250	8.	20.0		58.	42.	N
6387	4	2	SS	RE	1.15	100.	18.	.5000	8.	15.0		96.	70.	N
6387	4	5	SS	RE	1.15	100.	18.	.5000	8.	15.0		92.	67.	N
6387	5	2	AL	RE	0.89	200.	18.	.5000	8.	20.0		85.	61.	NG
6387	5	4	AL	RE	0.89	200.	18.	.5000	8.	20.0		116.	84.	NG
6387	5	5	AL	RE	0.89	200.	18.	.5000	8.	20.0		99.	72.	NG
6387	6	1	SS	RE	0.58	200.	18.	.3750	8.	15.0		92.	67.	N*
6387	6	2	SS	RE	0.58	200.	18.	.3750	8.	15.0		75.	55.	N*
6387	6	4	SS	RE	0.58	200.	18.	.3750	8.	15.0		78.	57.	N*
6387	6	5	SS	RE	0.58	200.	18.	.3750	8.	15.0		90.	65.	N*
6387	7	1	AL	RE	3.55	50.	-8.	.5000	8.	20.0		76.	55.	NR
6387	7	2	AL	RE	3.55	50.	-8.	.5000	8.	20.0		38.	28.	NR
6387	7	5	AL	RE	3.55	50.	-8.	.5000	8.	20.0		63.	46.	NR
6387	9	1	AL	RE	1.15	100.	-8.	.4375	10.	20.0		50.	36.	RR
6387	9	2	AL	RE	1.15	100.	-8.	.4375	10.	20.0		50.	36.	RR
6387	9	3	AL	RE	1.15	100.	-8.	.4375	10.	20.0		70.	51.	RR
6387	10	1	SS	RE	0.89	200.	-8.	.4375	10.	20.0		47.	34.	RR
6388	1	1	SS	RE		100.	-8.	.3750	6.	27.3		76.	56.	R
6388	1	2	SS	RE		100.	-8.	.3750	6.	27.3		119.	87.	R
6388	1	3	SS	RE		100.	-8.	.3750	6.	27.3		96.	70.	R
6388	1	4	SS	RE		100.	-8.	.3750	6.	27.3		100.	73.	R
6388	1	5	SS	RE		100.	-8.	.3750	6.	27.3		133.	97.	R
6388	2	1	AL	RE		100.	-8.	.3125	11.	20.0		53.	38.	RR
6388	2	2	AL	RE		100.	-8.	.3125	11.	20.0		44.	32.	RR
6388	2	3	AL	RE		100.	-8.	.3125	11.	20.0		51.	37.	RR
6388	2	4	AL	RE		100.	-8.	.3125	11.	20.0		63.	46.	RR
6388	2	5	AL	RE		100.	-8.	.3125	11.	20.0		53.	38.	RR
6388	4	3	AL	RE		200.	-9.	.3125	6.	27.3		89.	64.	RR
6388	4	4	AL	RE		200.	-9.	.3125	6.	27.3		65.	78.	RR

JO	RN	SN	CM	WG	WC	WS	T	IT	ST	DS	OC	OR	TAU	AF
6388	5	2	SS	RE		200.	-8.	.2500	11.	20.	0	57.	41.	RR
6388	5	3	SS	RE		200.	-8.	.2500	11.	20.	0	55.	40.	RR
6388	5	4	SS	RE		200.	-8.	.2500	11.	20.	0	46.	34.	RR
6388	5	5	SS	RE		200.	-8.	.2500	11.	20.	0	53.	38.	RR
6388	6	1	AL	RE		200.	-9.	.2813	15.	15.	0	30.	21.	RR
6388	6	2	AL	RE		200.	-9.	.2813	15.	15.	0	54.	39.	RR
6388	6	5	AL	RE		200.	-9.	.2813	15.	15.	0	53.	38.	RR

JO	RN	SN	CM	WG	WC	WS	T	IT	ST	DS	OR	FOR	TAU	TT
6389	1	1	SS	RE	2.61	100.	-8.	.3750	6.	27.		49.	36.	-8.
6389	1	2	SS	RE	2.61	100.	-8.	.3750	6.	27.		18.	13.	30.
6389	1	3	SS	RE	2.61	100.	-8.	.3750	6.	27.		21.	15.	33.
6389	1	4	SS	RE	2.61	100.	-8.	.3750	6.	27.		46.	34.	1.
6389	1	5	SS	RE	2.61	100.	-8.	.3750	6.	27.		64.	46.	1.
6389	2	1	AL	RE	2.61	100.	-8.	.2500	6.	27.		25.	18.	30.
6389	2	2	AL	RE	2.61	100.	-8.	.2500	6.	27.		8.	6.	30.
6389	2	3	AL	RE	2.61	100.	-8.	.2500	6.	27.		6.	4.	31.
6389	2	4	AL	RE	2.61	100.	-8.	.2500	6.	27.		2.	1.	32.
6389	2	5	AL	RE	2.61	100.	-8.	.2500	6.	27.		41.	30.	-3.
6389	3	1	SS	RE	1.77	100.	-8.	.2500	11.	20.		27.	19.	-5.
6389	3	2	SS	RE	1.77	100.	-8.	.2500	11.	20.		18.	13.	-5.
6389	4	1	AL	RE	1.77	100.	-8.	.6250	7.	20.		18.	13.	28.
6389	4	2	AL	RE	1.77	100.	-8.	.6250	7.	20.		12.	9.	28.
6389	4	3	AL	RE	1.77	100.	-8.	.6250	7.	20.		10.	7.	29.
6389	4	4	AL	RE	1.77	100.	-8.	.6250	7.	20.		29.	21.	25.
6389	6	2	AL	RE	1.77	100.	-8.	.6250	7.	20.		49.	36.	25.
6389	6	3	AL	RE	1.77	100.	-8.	.6250	7.	20.		16.	12.	28.
6389	6	5	AL	RE	1.77	100.	-8.	.6250	7.	20.		47.	34.	-8.

1. Report No.	2. Government Accession No.	3. Recipient's Catalog No.
NASA CR-179580		

4. Title and Subtitle	5. Report Date
Structural Properties of Impact Ices Accreted on Aircraft Structures	January 1987
	6. Performing Organization Code

7. Author(s)	8. Performing Organization Report No.
R.J. Scavuzzo and M.L. Chu	None
	10. Work Unit No.
	505-68-11

9. Performing Organization Name and Address	11. Contract or Grant No.
The University of Akron Mechanical Engineering Department Akron, Ohio 44325	NAG3-479
	13. Type of Report and Period Covered

12. Sponsoring Agency Name and Address	Contractor Report Final
National Aeronautics and Space Administration Lewis Research Center Cleveland, Ohio 44135	14. Sponsoring Agency Code

15. Supplementary Notes

Project Manager, William A. Olsen, Propulsion Systems Division, NASA Lewis Research Center.

16. Abstract

The structural properties of ice accretions formed on aircraft surfaces are studied in this investigation. The overall objectives of the project are to measure basic structural properties of impact ices and to develop finite element analytical procedures for use in the design of all deicing systems. The Icing Research Tunnel (IRT) at the NASA Lewis Research Center was used to produce simulated natural ice accretion over a wide range of icing conditions. Two different test apparatus were used to measure each of the three basic mechanical properties: tensile, shear (adhesion), and peeling. Data has been obtained on both adhesive shear strength of impact ices and peeling forces for various icing conditions. The influences of various icing parameters such as tunnel air temperature and velocity, icing cloud drop size, material substrate, surface temperature at ice/material interface, and ice thickness were studied. A finite element analysis of the shear test apparatus was developed in order to gain more insight in the evaluation of the test data. A comparison with results of other investigators is made. The result shows that the adhesive shear strength of impact ice typically varies between 40 and 50 psi, with peak strength reaching 120 psi and is not dependent on the kind of material substrate used, the thickness of the accreted ice, and tunnel temperature below 4 °C (25 °F). For temperature above 4 °C (25 °F) the shear strength is found to (a) decrease sharply with rising ice/material interface temperature (down to 0.0 psi at 0 °C (32 °F)) and to (b) increase slightly with the increase in wind velocity and drop size. The peeling strength is found to be extremely low at high peel angles. The values vary from 3 to 5 lb/in. for both neoprene and stainless steel substrate.

17. Key Words (Suggested by Author(s))	18. Distribution Statement
Structural properties of ice Aircraft icing	Unclassified – unlimited STAR Category 39

19. Security Classif. (of this report)	20. Security Classif. (of this page)	21. No. of pages	22. Price*
Unclassified	Unclassified	58	A04

*For sale by the National Technical Information Service, Springfield, Virginia 22161